# Strike-slip overprinting of initial co-axial shortening within the toe region of a submarine landslide: a case study from the Angoche Basin, offshore Mozambique.

Clara Abu[1*], Christopher A-L. Jackson[1], Malcolm Francis[2]

[1]Basins Research Group (BRG), Department of Earth Science & Engineering, Imperial College, London, UK

[2]WesternGeco, Schlumberger House, Buckingham Gate, Gatwick, UK

*corresponding author: clara.abu07@imperial.ac.uk

## Abstract

Submarine landslides (slides) are some of the most voluminous sediment gravity-flows on Earth and they dominate the stratigraphic record of many subaqueous basins. The general kinematics and internal structure of slides are relatively well-understood, although the way in which they increase in volume and internally deformed as they evolve, and how these processes relate to the development of their basal (shear) surface, remains largely unknown. We here use three high-resolution 3D seismic surveys (two broadband time-migrated seismic reflection datasets and a depth-migrated volume) from the Angoche Basin, offshore Mozambique to undertake detailed mapping and intra-slide strain analysis of a shallowly buried, large, and thus well-imaged submarine landslide (c. 530 km$^3$). We also provide detailed documentation of the along-strike variations in the structural style and evolution of the toe region, and how these relate to the overall emplacement of the slide. Seismic attribute analysis image several key kinematic indicators, including broadly NW-trending (i.e., flow-parallel) lateral margins, longitudinal shears, and sub-orthogonal shears in the main body of the deposit, and broadly NE-trending (i.e., flow-normal) symmetric pop-up blocks in the toe region. The slide exhibits varying degrees of frontal emergence along strike, displaying a single frontal (toe) wall in the SW to a more complex, stair-step geometry in the NE. Basal grooves are noticeably absent, with a key observation being that contractional structures are locally observed c. 7 km downdip of the present toe wall. Based on the distribution of and cross-cutting relationship between intra-slide structures, we propose an emplacement model involving two distinct phases of deformation; (i) bulk shortening, parallel to the overall SE-directed emplacement direction, accommodated by the formation of NE-trending symmetric pop-up blocks bound by fore-thrusts and back-thrusts; and (ii) the development of NW-trending sinistral shear zones that offsets the earlier formed shortening structures, and which possibly formed due a spatial variations the evolving rock strength as the flow arrested, resulting in intra-slide flow cells. We infer the basal shear surface or zone incrementally propagated downdip *ahead* of the developing slide mass, with distal contractional structures being the expression of rather cryptic, updip sliding of the entire sediment mass. Our study demonstrates the value of using 3D

seismic reflection data to study the structure and emplacement kinematics of slides, and the complex strains that can arise due to temporal and spatial variations in sediment rheology.


# 1. Introduction

Submarine landslides are subaqueous sediment gravity-current deposits, emplaced by a range of creep, slide, slump, and debris flow processes (e.g. Dott 1963; Nardin 1979; Nemec 1990; Weimer 1990; Posamentier and Martinsen 2011). Submarine landslides are commonly sourced from the outer shelf and middle-to-upper slopes of submarine and lacustrine basin margins, or the flanks of salt domes, mud volcanoes, and subaqueous channel levees. Submarine landslides are largely mud-prone, although those sourced from sand-rich shelf-edge deltas may by relatively sand-prone (Posamentier and Martinsen 2011; Wu et al. 2019). Slope instability triggers slide emplacement; this instability can be promoted by slope oversteepening, cyclic waves, seismic activity, lowering of wave base, and overpressure development related to fluid expulsion (Bull et al. 2009a; Posamentier and Martinsen 2011).

Submarine landslides are commonly defined by a tripartite morphology comprising upslope (head), an intermediate (translational), and downslope (toe) zones (e.g. Brunsden,1984; Gawthorpe and Clemmey, 1985; Martinsen, 1989, Posamentier and Martinsen 2011). Extensional strains, typically manifest as normal faults, dominate the head zone, whereas contractional structures are common in the toe zone. The toe zone of a submarine landslide can be further sub-divided based on the mode of frontal emplacement (Frey-Martinez et al. 2006); (1) *frontally confined slides* – these are characterized by a translated mass that is fully buttressed downslope against the downslope toe wall, which results in the development of downslope-verging fold-and-thrust systems that trend normal to the emplacement direction and (2) *frontally emergent slides* – these are characterized by a failed mass that ramps up and is expelled beyond the toe wall onto the seafloor (Frey-Martinez et al. 2006), resulting in the formation of pressure ridges (e.g. Prior et al.1984; Frey-Martinez et al. 2006) that likely reflect sub-seismic folds and thrusts (Bull et al. 2009a). Outcrops datasets provide critical information on the structural style and processes occurring within the toe zone of submarine landslides, but these are often limited in their areal extent and three-dimensionality (Martinsen and Bakken 1990; Van Der Merwe et al. 2011; Ogata et al. 2012; Sobiesiak et al. 2016; Cardona et al. 2020). As such, it is difficult to put these observations in the larger-scale context of the host slides, i.e., how does the observed local strain relate to the overall transport direction and magnitude of the larger host slide? This context is most readily provided by 3D seismic reflection datasets, which reveal the general seismic expression and kinematics of the end-members styles present in submarine slide toe zones; however, only few 3D seismic reflection-based studies have provided a detailed documentation of the along-strike variations in the structural style and evolution of the basal shear surface in this zone (i.e. the surface underling an slide; e.g. Bull et al. 2009a; Nugraha et al. 2020). Quantitative assessment of intra-slide strain has also only rarely been investigated using 3D seismic reflection data (e.g. Steventon et al. 2019; Bull and Cartwright 2019). As a result, we have a relatively poor understanding of the detailed processes occurring within the toe zone of submarine landslides and related to this, how slides increase in volume via basal shear surface propagation (Martel, 2004; Hodgson et al. 2019).

The translational zone is often thought to be dominated by pure translation with little internal deformation. This may not always be the case. For example, along-strike variations in the rate of downslope translation of a failed sediment mass can lead to the formation of flow cells, separated by regions of discrete (i.e. strike-slip faults) or diffuse (i.e. shear zones) deformation. Such cells have been documented in the field at the cm- to m-scale, but it is often not explicitly clear how they relate to overall kinematics of the deposit in which they are hosted, or indeed where or when they form within the failed mass (Farrell 1984; Alsop and Marco 2014). 3D seismic reflection data can address these shortcomings, showing that flow cells form within the translational zone in response to variations in the downslope translation of the failed sediment mass (Gee et al. 2005; Bull et al. 2009; Steventon et al. 2019).

Here we use high-resolution 3D time-migrated seismic reflection data imaging an area of c. 4765 km$^2$ of the Angoche Basin, offshore Mozambique to undertake detailed mapping and strain analysis of a shallowly buried, large, and thus well-imaged submarine landslide (c. 530 km$^3$). The 3D seismic reflection dataset fully covers the toe domain of the deposit, which therefore forms the focus of this study. We show that the submarine landslide exhibits varying degrees of frontal emergence, with the basal shear surface passing from a single major frontal (toe) wall in the SW to a more complex, stair-step geometry in the NE. Seven kilometres basinward of the north-western part of the toewall, in relatively undeformed slope strata, are subtle but clearly imaged thrusts and related folds; we infer that these sit above the cryptic basinward extension of the basal shear surface underlying the main slide body and with additional strain, would become part of the larger failed mass. We also show that in contrast to the development of classic, downslope-verging, asymmetric fold-and-thrust belts, the toe region is characterised by broadly symmetric, NE-trending pop-up blocks that are bound by forethrusts and backthrusts. Cross-cutting relationships indicate the toe region underwent two distinct phases of deformation; (1) bulk shortening, parallel to the overall SE-directed emplacement direction, accommodated by the formation of thrust-bound pop-ups; and (2) the development of NW-trending sinistral shear zones that offsets the earlier-formed structures (Frey-Martinez et al. 2005; Reis et al. 2016; Alsop et al. 2017; Steventon et al. 2018). We suggest that as it translated, the toe zone of the slide mass compacted via pore space collapse and the extrusion of pore water, causing sediment embrittlement and, ultimately, the development of seismic-scale contraction structures. This process was spatially variable, possibly due to lateral changes in sediment porosity, pressure build-up, and the evolving rock strength, leading to the development of intra-slide flow cells and bounding shear zones, the former traveling downflow at speeds and/or at slightly different times.

## 2. Geological Setting

The offshore basins in Mozambique initially formed during the early Mesozoic in response to the break-up of Gondwana (Mahanjane 2014). The Angoche Basin (Fig. 1) is bounded to the west by the Mozambique continental margin and the Davie Fracture Zone in the east. Rifting occurred in two key stages related to: (a) dextral strike-slip movement parallel to the present coastline, followed by initial sea-floor spreading, probably in the Middle Jurassic (Bajocian-Bathonian, 170-166 Ma), and (b) Late Jurassic phase (154 Ma) rifting between West and East Gondwana, which was associated with the north-south directed extension that created the Davie Fracture Zone and the Lebombo Monocline (Reeves and Mahanjane 2013).

The sedimentary succession offshore Mozambique is several kilometres thick. Synrift lacustrine deposits of the Makarawe Formation were deposited during the Middle Jurassic (Bajocian), with overlying uppermost Jurassic post rift deposits comprising marine shales and siltstones deposited in shallow-marine conditions (Sapri et al. 2013). Deeper-water conditions and related deposits characterise the overlying Cretaceous succession ( Francis et al. 2013; Mahanjane and Frank 2014). A marine transgression during the Cenozoic (Salman and Abdula 1995), in conjunction with Tertiary uplift of East Africa, resulted in an increased sediment flux into the basin and the deposition of deep-water channels and fan systems above a largely mudstone-dominated Paleogene package. Renewed rifting in East Africa destabilised the Mozambique Shelf during the Oligocene and Neogene (Fig. 3), leading to the emplacement of thick extensive, submarine landslides. One of these slides forms the focus of this study (Fig. 2)

# 3. Dataset and methods

## 3.1 Dataset and seismic interpretation

The data used in this study consist of three 3D seismic surveys; two broadband time-migrated (PSTM) seismic reflection datasets that cover areas of c. 15,041 $km^2$ and c.4765 $km^2$, and a depth-migrated volume that covers 2545 $km^2$. The time-migrated datasets are processed differently, with the larger survey having an inline spacing of 12.5 and crossline spacing of 25 m, whereas the smaller survey has an inline spacing of 6.25 m and crossline spacing of 12.5 m; we use the former to define the overall geometry and kinematics of the studied slide, whereas the latter is used to undertake a detailed analysis of the slide toe region. The dominant frequency of the data varies with depth but is c. 60 Hz for the interval of interest. Depth interval velocities for the sediment are taken from models updated by advanced full-waveform inversion (FWI) and common image point (CIP) tomography. From this we derive an average seismic velocity of 1935 ms-1 for the interval of interest, giving a maximum vertical resolution of c. 8 m (wavelength $\lambda$ = V/f, m; maximum vertical resolution = $\lambda/4$; Sheriff and Geldart 1983), and a horizontal resolution of c. 32 m. The data are SEG standard polarity with an increase and decrease in acoustic impedance represented by a peak (blue) and a trough (red), respectively.

We focus on a well-imaged slide located 620 ms to 3637 ms (c. 599-3483 m, using average slide velocities of 1935ms-[1]) beneath the seabed (Fig. 2). Water depths increases from 0.45 s (336 m) in the northwest to >3 s (2242 m) in the southeast. For depth conversion, the water layer was defined using a depth-variant water-velocity. We mapped the top and base of the slide to constrain its structural style and infer its emplacement kinematics. Isoproportional horizons are also created halfway (see Zeng et al. 1998) between the top surface and the basal shear surface to reveal the internal structural characteristics of the slide, from which we infer its emplacement kinematics.

## 3.2 Seismic attribute analysis

Several seismic attributes reveal the internal and external geometry of the studied slide: (i) the *variance attribute* (Van Bemmel et al., 2000) isolates edges and discontinuities in the horizontal continuity of amplitude, and hence accentuates structural features (e.g. faults) within the slide; note that the variance attribute is used as an input to the ant-tracking workflow; (ii) *ant-tracking* performs edge enhancement (or skeletonization) for identifying faults, fractures, and other linear

anomalies within the seismic data volume (Pedersen et al., 2002); (iii) *eXchroma*, a method adapted from processing of satellite images for geology, allows a simultaneous rendering of several slices or layers in continuous RGB colours. In our case, subsequent image processing enhances the contrast of the RGB images to reveal the internal geometry of the slide in detail; (iv) *dip illumination*, which uses a cross-correlation dip estimation method to reveal structural discontinuities (e.g. faults) in the seismic data and to help image the rugosity of a mapped seismic horizon (v) *root mean square (RMS)*, a statistical measure of reflectivity or energy in a dataset; this helps highlight isolated geologic features such as reflective megaclasts contained within the low-amplitude debritic matrix of the slide (e.g. Ortiz-Karpf et al. 2017); (vi) *amplitude contrast* is a Sobel-based attribute computation of the amplitude derivatives between neighboring traces, followed by a normalization of the calculated differences. Surface-based amplitude extractions involved windowed extractions above, below or on specific horizons. Iso-slicing within the slide allows an examination of the internal morphology of the slide.


## 3.3 Strain analysis
**Shortening calculation**
We use the well-established line-length method (e.g. Dahlstrom 1969; Totake et al. 2018; Bull and Cartwright 2019; Steventon et al. 2019) to calculate shortening and investigate longitudinal strain within the toe region. We apply this method to a representative depth section, taken parallel to the dominant transport direction of the slide. This was dependent on identifying kinematic indicators using a combination of time structure maps, seismic sections, and extracted attribute maps (see Appendix). The shortening values of the pre-kinematic strata of the fold and thrust systems are estimated by comparing the present length (Lf) with the cumulative length of the pre-kinematic horizon (Li) (Eq. 1):

$$e = (Lf - Li)/Li$$

This estimation provides minimum shortening values without accounting for sub-seismic strain shortening and porosity loss due to dewatering and/or grain crushing (e.g. Alsop et al 2019; Steventon et al 2019).


**Along-strike variation in structural style**
Thrusts and thrust bound pop-up blocks in the contractional part of the toe region are highly segmented along-strike. We focus on a relatively large (7 km strike length), well-imaged set of contractional features, measuring the throw of thrust bounding contraction-related pop-up blocks every 50-150 m along-strike. Throw is plotted against the along-strike distance, allowing us to infer the kinematics of contractional structures in the toe domain (see Nugraha et al., 2020).

# 4. Seismic characterization of the slide

## 4.1 General characteristics

The slide has a maximum depositional length of c. 85 km (Fig. 2), an area of 3746 km$^2$, a maximum thickness of c. 447 ms (380 m), and a total volume of c. 530 km$^3$. It is c. 46 km wide in its central part and narrows downdip to c. 26 km in its toe region (Fig 5). The slide is dominated by low-amplitude, chaotic seismic reflections and it overlies a high-amplitude reflection that is broadly concordant with underlying stratigraphy. The high-amplitude basal reflection is interpreted as a basal shear surface or zone, across which the slide was translated (e.g. Frey Martinez et al. 2005; Bull et al. 2009a; Wu et al. 2021). The basal shear surface passes upslope into a headwall scarp zone that defines the updip limit of the slide, and downslope into a frontal ramp that defines the contractional part of the slide. The basal shear surface cuts up through stratigraphy to define the slides lateral margins (see below); beneath the slide, relief along the basal shear surface defines a series of ramps. The basal shear surface largely exhibits a negative continuous reflection polarity but becomes discontinuous where ramps are present and locally discordant to underlying stratigraphy.

The slide terminates across-strike against a lateral margin (Figs 4b-c) that trends parallel to the gross SE-directed emplacement direction. The lateral margin is easy to trace downslope, being defined by a clear, linear, steep, continuous scarp that is up to 300 ms high and ultimately links to the frontal ramp in the toe domain (Fig 5b). The lateral margin is locally flanked by en echelon tension cracks, such as in the NW part of the toe domain. The en enchelon faults links to form a through-going fracture in the SW of the toe region and records strike-slip movement (Martinsen and Bakken, 1990; Martinsen, 1994; Frey-Martinez et al., 2005).

The top of the slide is rugose and has a vertical relief of up to 989 ms (957 m). The slide is thickest and has greatest relief in the SW, where thrusts and thrust-bound pop-up blocks are common and expressed as positive relief ridges on the slide top surface. Across much of the study area, the top surface has a positive reflection that defines a downward increase in acoustic impedance. Locally, however, such as the distal parts of the toe domain, it has highly variable reflectivity or a discrete reflection is absent. The variable in the acoustic expression of the top surface at its toe domain could reflect the variable physical properties (e.g. density, velocity) of materials within and above the slide. A chaotic seismic facies fills the depressions between thrust-cored folds and shear zones in the toe region of the slide. Steventon et al. (2019) describes similar supra-slide deposits offshore Uruguay, interpreting that the bounding package, which ultimately thins basinward within the frontally emergent zone, as a mud-rich debrite.

The toe domain of the slide has a clear arcuate, convex-towards-the-direction-of-transport geometry. We see the development of thrust-related folds that are hundreds of meters wide and laterally extensive; strike variability in frontal ramp geometry and development of shear zones (more detailed descriptions of these and the shear zone-like structures are discussed below in the toe domain).

## Description and interpretation of slide seismic facies

The internal seismic and structural character of the slide is highly variable, so we develop a seismic facies classification scheme to help with our description. Our scheme is largely based on previous ones developed from the analysis of shallowly buried, undrilled slides that are well-imaged in 3D seismic reflection data, and more deeply buried slides that have been drilled and for which direct lithological data are available (Wu et al. 2021). Various techniques are utilized including dip-oriented vertical seismic sections, horizon slices, and proportional slices from an RGB display extracted between the basal shear surface and the top surface (Figs 6b, 7).

We define three seismic facies in this study based on the changes in the internal configuration of the reflections, in cross-section and map-view (Table 1, Fig. 7c-e). (i) SF1 – very low-amplitude, chaotic reflections, inferred to be the slides debritic matrix (e.g. Posamentier and Kolla 2003; Posamentier and Martinsen 2011; Olafiranye et al. 2013; Alves et al. 2014; Ortiz-Karpf et al. 2017; Nugraha et al. 2019). (ii) SF2 – variable to high-amplitudes reflections that are folded and offset by thrusts (e.g Bull et al. 2009; McGilvery et al., 2004; Frey-Martinez et al. 2005; 2006; Alfaro & Holz, 2014), interpreted as imbricate thrust and fold systems, and (iii) SF3 – high-amplitude isolated blocks of coherent, parallel, weakly-to-moderately folded reflections that are set within an inferred debritic matrix (e.g. SF1-2) and which are interpreted as megaclasts (e.g. McGilvery et al. 2004; Bull et al. 2009; Frey-Martinez 2010; Jackson 2011; Posamentier and Martinsen 2011; Olafiranye et al. 2013; Ortiz-Karpf et al. 2015; Alves 2015).

## 4.2 Toe Domain
### Basal Shear surface
The basal shear surface steepens downdip below the slides toe region, connecting to a steep ramp that defines the slides frontal ramp and the downdip limit of the contractional domain. In map-view, the frontal ramp is broadly perpendicular to the gross transport direction and has a complex morphology (Fig. 9). In the SW, it is defined by a c. 230 ms-high frontal ramp, with the basal shear surface being deepest immediately adjacent to the frontal margin (Fig. 9). To the NE, however, the frontal ramp has a more complex, stair-case or ramp-flat-ramp-like geometry, consisting of two steep-dipping walls separated by an intermediate, strata-parallel detachment (Fig. 10a-b). There is considerable variation in relief (up to 450 ms) along the basal shear surface due to the presence of steps and ramps. In both the NE and SW the slide's basal shear surface ramps up onto the seabed, with a relatively thin veneer of the overlying sliding mass being present basinward of this point, deposited on relatively undeformed basin floor substrate. The slide falls therefore into the frontally emergent termination style (*sensu* Frey-Martínez et al. 2006). Further downdip but still within the toe zone, we observe SE-trending, linear grooves on the basal shear surface (Fig. 8).

### Internal body
#### *Shortening-related structures*
The contractional domain is highly deformed by a range of shortening-related structures. Well-imaged thrust-bound pop-up structures are common, occurring in arcuate belts that trend broadly

N in the NE of the deposit, and E and in the SW of the deposit. A slice through a product of variance and ant-tracking attribute reveals remarkable pattern of sub parallel EW trending lineations at the distal end of the toe (Fig 9). The continuous lineations in map-view correspond to reflection discontinuities in vertical seismic sections (Figs. 11 and 12) and correspond to forethrusts (i.e. N-dipping) and back-thrusts (i.e. S-dipping).  The average throw and dip of the fore- and back-thrusts are c. 60 m and c. $40 - 50^0$ (some up to $> 55^0$), respectively. Spacing between thrust pairs (measured from crest to crest of the pop-up blocks) range from 460 to 805 m. The height of the thrust's ranges from 150 – 200 m (Fig. 14a). The oppositely dipping thrusts bound regularly spaced pop-up structures with maximum displacements of up to c. 130 ms detaching downwards onto the basal shear surface. The thrust faults define a horizontal shortening perpendicular to the minimum compressive stress, suggesting a transport (and slide emplacement) direction perpendicular to the strike of the thrust faults (i.e. broadly towards the SE; Ramsey and Lisle 2000). Thrusts bound upright folds that define pop-up blocks. The folds are gentle, non-cylindrical and affect sections as thick as 370 ms, for example just updip of the toe zone ramp. The fold axes are mostly NE-SW, sub parallel to the strike direction, again indicating a gross slide transport direction towards the SE.  The thrust-and-fold system (i.e. SF3; Table 1 and Fig. 9) is best-developed in the distal part of the toe domain (Fig 7b).

The toe region is subdivided into two parts: an inner thrust-belt and an outer thrust-belt (Fig. 6b). The inner thrust-belt is dominated by symmetrical, thrust-bound pop-up blocks, within which internal reflections are relatively well-preserved. These internal reflections are similar in terms of overall seismic character to adjacent, undeformed strata, located outside of the slide body. The outer thrust-belt is characterized by so-called pressure ridges (*sensu* Bull et al. 2009a) that are most evident in the SE part of the toe domain. Pressure ridges are inferred to be an expression of thrusts below the resolving power of seismic reflection data (Bull et al. 2009a). These ridges are linear-to-arcuate (convex-downslope) in plan-view and trend perpendicular to the overall south-easterly emplacement direction.

### Shearing-related structures

Several downslope-trending lineaments are developed within the toe region of the slide. The shear zones have a range of orientations and crosscut and offset the thrust-bound pop-up blocks described above (see dotted lines on Fig. 9). The shear zones cross-cut the entire height (i.e. up to 400 ms (387 m)) of the slide even, although their expression along the top surface is very subtle, possibly due to the presence of overlying in the uppermost part of the slide. The shear zones are very narrow (up to 100 m wide) zones that are defined by chaotic seismic facies, that might have been derived from the overriding debrite. We identify three main groups of shear zones based on their orientation: slope-parallel shears 'longitudinal' (NW-SE), slope-oblique shears 'sub-orthogonal' (N-S) and slope orthogonal (NNE-SSW) (Fig. 9). Orthogonal shear zones are smaller and common downslope in the toe zone, whereas the slope-parallel and oblique shears are laterally extensive.

# 5. Strain distribution in the toe region

## *Shortening*

We estimate the shortening magnitude of the submarine landslide based on a line-length method-based assessment of shortening using a depth-migrated seismic line that trends NW within the toe region and that has a good preservation of internal reflections. This distance however reflects the minimum distance travelled by submarine landslide in the toe region (Frey-Martínez et al. 2006). The line is almost perpendicular to the trend of the pop-up blocks. We interpreted an intra-slide horizon (H1) to constrain the extent of horizontal shortening; this horizon extends from an area with little deformation to an updip section in the toe region of the slide. Our analysis shows present and restored lengths of H1 of 12.39 km and 13.43 km, respectively, which equals contractional shear strains (as expressed and accommodated by seismically imaged thrusts) of c. 8%.

## *Along-strike strain variability*

We also quantify the intra-slide strain of a pop-up block within the same area to investigate how strain varies along-strike, and to infer how structures grow during progressive shortening (see Nugraha et al. 2020).

The along-strike variability in strain is calculated for the tenth block from the frontal margin, hereafter called PB10, and its bounding fore- and back-thrusts. This pop-up block (Figs. 14 a and b) is used for analysis because the main bounding thrust (FT1) and horizon H1 can be interpreted over a relatively long distance (7 km) along-strike

## *Throw profiles*

The seismic sections across PB10 show the change in pop-up block configuration along strike from the SW to the NE (Fig. 15a-c). In the SW, PB-10 is defined by a single pop-up block bound by forethrust FT1 and backthrust BT1 (Fig. 15a), passing along-strike to the NE into two pop-up blocks bounded by two forethrusts (FT1, FT2) and two backthrusts (BT1, BT2) (Figs 14a and 15c). One of the shear zones described above trends oblique to, crosscuts, and offsets the pop-up and bounding thrusts in the SW, demonstrating sinistral offset c. 60 m of the presumably older shortening-related structure (Fig. 14a).

The throw vs. distance (T-x) profiles for the pop-up-bounding thrusts have irregular shapes (Fig 14c). The T-x plot for FT1 shows an overall bimodal throw profile, defined by a throw minimum of c. 25 m, located c. 3500 m along-strike. Maximum throw is slightly lower on the SW segment (c. 55 – 60 m) than the NE segment (c. 70-85 m). We note that there is no major change in throw across the shear zones. The T-X plot for BT1 shows a similar throw profile to FT1. The throw profile highlights that along strike to the NNE, there are more thrusts. The deficit in throws in FT1 and BT1 are balanced by FT2, BT2 and BT1X.

## *Interpretation*

We interpret two shear zones within the chosen area of analysis - oblique and orthogonal shear zones (i.e. described in the shearing-related structures of the toe domain and highlighted by the green dotted lines in Fig. 14a). The seismic facies separated by these shear zones are probably

transported by a similar distance although there are more thrusts in the north east than in the south west (Fig. 14a).

The throw profiles of the individual fore and back-thrusts are similar to large-scale thrust systems, such as those found offshore NW Borneo (Totake et al. 2018). The cumulative throw plot on pop-up-bounding thrusts suggests similar throws between backthrusts and forethrusts and that strain is broadly balanced.

# 6. Slide trigger and emplacement mechanisms

Having described the seismic expression and structure of the slide, we now consider how it was triggered and the processes involved in its emplacement. We note that the slide is overlain by a chaotic seismic-stratigraphic package interpreted as a debrite. This stratigraphic relationship suggests three potential end-member scenarios for the triggering and evolution of the slide: (1) the passage of the debrite initiates failure and deformation of the underlying substrate (e.g. Hodgson et al. 2019), (2) loading and subsequent downslope failure followed by later infilling by debrite and (3) pore pressure build-up along a discrete layer in slope sediments results in a reduction of shear strength and initiates slope failure and slide formation.

Scenario 1 envisages that slope failure was triggered by the passage of an overriding debris flow, which caused the critical shear stress of the substrate to be exceeded, and the propagation and growth of the basal shear surface along subsurface bedding planes (Watt et al. 2012). This causal link between debrite emplacement and slide triggering is inferred from 3D seismic reflection (e.g. Moscardelli et al. 2006; Hodgson et al. 2019) and field data from the Karoo Basin, South Africa (Van der Merwe et al. 2011). For example, Van der Merwe et al. (2009) demonstrate substrate deformation by the development of an underlying slide due to high basal shear stresses and vertical loading stress from an over-riding debris flow; in this case, the relatively thick slide essentially formed part of a basal shear *zone* rather than *surface* (e.g. Butler et al., 2010; Wu et al., 2021). Debris flow-driven shear coupling is also proposed as an explanation for the development of large-scale mass transport deposits (Schnellmann et al. 2005; Minisini et al. 2007; Dasgupta 2008). The following observations broadly support scenario 1: (1) strong erosional scouring (e.g., grooves) is absent at the base of the slide, suggesting it has only translated a short distance; (2) thrust-cored folds in the distal domain are capped by but not eroded into by the overlying debrite; and (3) the debrite has the same map-view extent as the slide itself. However, the slide studied here has a total volume of c. 530 km$^3$, with a c. 3:1 thickness ratio between the relatively thick slide (c. 300 ms) and relatively think debrite (80-100 ms). It is not therefore clear if a relatively thin flow could cause such sufficient loading of the substrate to trigger such a volumetrically large failure along a deep-lying bedding plane (see also discussion by Steventon et al., 2019).

Scenario 2, like Scenario 1, also view the slide and debrite as being genetically related. However, in this case, it is the formation of the slide that triggers the formation of a debris-flow, not the other way around. More specifically, having been triggered due to slope failure, the upper part of the slide ingests water, becomes more dilate, and transforms to a debris flow. Both the slide and the debris flow progress seaward, with the former ploughing and incorporating the material ahead of it, forming folds and thrusts (Fig.18). It suggests that slope failure and slide triggering occurred due to pore pressure build-up along a discrete layer or closely spaced layers in the slope sediments;

this reduced the frictional and related shear strength of this interval, such that the normal stress induced by the weight of the overburden was overcome, resulting in shear failure and slide emplacement (e.g. Martel 2004). Landsliding involves upslope depletion, downslope translation and base-of-slope accumulation of a sedimentary mass that abandons its initial failure region to form a positive topographic feature on the seafloor. Initially developed by Farrell (1984) and subsequently modified by Martel (2004), the model suggests sliding nucleates at depth over a small region along a discrete surface, with stress concentrations at the edge of this region driving propagation of the plane as a shear fracture (Martel 2004). Shear fracture deformation at depth precedes large displacements in the slide mass, which ultimately lead to extension and contractional structures in the head and toe domain, respectively (see below). The following observations supports scenario 2: (1) observation of contractional structures ahead of the flow and entrainment of large fragments from seabed as the debrite flowed (Fig. 16). (2) Progressive imbrication downslope and the formation of regularly spaced pop-up blocks bounded by thrust planes. A similar model is proposed by Sammartini et al. (2021) using examples from the Zinnen Slide, Lake Lucerne, Switzerland, in which debrite and slide emplacement are coeval. They suggest the initiation and growth of shear bands along discrete decollements on steep slopes that permit the basinward propagation of the deformation. The landslide evolves as two bodies, a debrite and a coherent slide that ploughs into basin sediments, ultimately generating compressive stress and a deformation front that leads to the formation of folds and thrusts.

In contrast to scenarios 1 and 2, Scenario 3 envisages that the slide and debrite are genetically *unrelated*. Instead, this scenario suggests that loading of sediments drives pore pressure buildup, reduction of sediment strength, and ultimately slope failure. In this scenario, relief along the top of the slide is later and passively filled by a younger debrite, although the top of the former might be eroded into by the latter. This stratigraphic relationship has recently been described from Lake Lucerne, Switzerland (Sammartini et al. 2021). The authors report that a mass flow superficially eroded fold-and-thrusts developed in an older, underlying slide, with the magnitude of erosion decreasing downdip. Such erosion locally occurs in the NE of the deposit (Fig. 15).

**Basal shear surface evolution**

In the three proposed scenarios, the development of a basal shear surface or zone is a fundamental process. Such surfaces or zones can occur along pre-existing planes of weakness (e.g. bedding surfaces), or along or just below (i.e. due to overpressure development) clay-rich intervals. Several studies depict this surface as being developed in or at the top of contourite deposits (Bryn et al. 2005), hemipelagic (Frey Martinez et al. 2006), or glacial (Sammartini et al. 2021) deposits. In seismic reflection data the basal shear surface or zone is often expressed as a distinctive, commonly high-amplitude seismic reflection that is concordant to or strongly discordant with, underlying stratigraphy. Although mappable over large areas, the mechanisms responsible for the propagation of the basal shear surface or zone during slide evolution is very poorly understood.

Our data allows us to analyze how the basal shear surface or zone developed. Here we consider a simple mechanical explanation proposed by Martel (2004) originally for subaerial landslides. In this model the surface at the base of a slide is considered a slope strata-concordant shear fracture, with localized stress concentrations occurring near the perimeter of the region undergoing shear dislocation (i.e., sliding). The failing slide exerts significant in-plane stress concentrations and

lateral compressional stress against flanking slope sediments, causing the development of contractional structures (e.g., thrusts) in the toe region that nucleate on the evolving basal shear surface or zone, and which propagate upwards into overlying sediments. These discrete structures may be associated with related folds. The critical aspect of this model is that shearing, sliding, and basal shear surface or zone formation precedes significant deformation of the overlying sediment mass

We argue this model can describe the styles and patterns of deformation observed here, given contractional strains (e.g., thrusts and folds) clearly developed c. 7 km downslope of the current toe wall. Critically, the related structures are geometrically similar (but simply less numerous) than those within the main slide mass, detaching downwards onto the downslope continuation of the basal shear surface or zone underlying the slide body (Fig. 16). We therefore infer that the entire sediment mass between the slide toe wall and the downdip limit of contractional strains beyond the toe wall have undergone cryptic lateral translation. The relatively weakly deformed strata in this region is essentially a giant megaclast. Only a few hundreds of metres of lateral movement is required to account for the magnitude of contractional strains (e.g., thrust-related stratigraphic overlap or heave) observed downdip, with such a modest amount being consistent with the lack of erosional features (e.g., grooves) along the slide base. We therefore propose a model by which the basal shear surface or zone incrementally propagates downdip *ahead* of the developing slide mass, with material above this level being translated and possibly shortened before being incorporated into the main body of the evolving slide (Figs. 16 and 17). A similar mechanism, which involves the plucking of megaclasts from a dynamically deepening basal shear surface is proposed by Ortiz-Karpf et al. (2017) based on their analysis of 3D seismic reflection data form offshore Colombia.

# 7. Discussion

### Lateral variability in frontal confinement in the toe region

Contractional strains typically dominate the toe region of slides due to buttressing of the translating sediment mass against the frontal toe wall (Frey-Martinez et al. 2006, Bull et al. 2009a; Posamentier and Martinsen 2011). In the example presented here, this strain is recorded by the formation of NE-SW striking thrusts and pop-ups, which constitutes the first phase of deformation. The pop-ups differ to those previously documented in similar slides (Suppe and Medwedeff, 1990; Frey-Martínez et al. 2006; Bull and Cartwright 2019; Nugraha et al. 2019) in that they are symmetrical and not strongly asymmetrical, suggesting minimal shearing through folds.

The toe zone of slides are broadly classified into two end-member models based on the mode of frontal emplacement (Frey-Martinez et al. 2006); (1) frontally confined slides are characterized by a translated mass that is fully buttressed downslope against the downslope toe wall, which results in the development of downslope-verging fold-and-thrust systems that trend normal to the emplacement direction and (2) frontally emergent slides are characterized by a failed mass that ramps up and is expelled beyond the toe wall onto the seafloor (Frey-Martinez et al. 2006) and exhibits pressure ridges (e.g. Prior et al.1984; Frey-Martinez et al. 2006).

Trincardi and Argnani (1990) argue that the frontal confinement of the Gela Landslide relates to the presence of a morphostructural obstacle that restricted further basinward motion.  Huvenne et

al. (2002) postulate that confined landslides resulted from a combination of abrupt pore-pressure dissipation from the basal shear surface and a low regional slope angle. Frey Martinez et al. (2006) argue that the depth to the basal shear surface effectively determines the cross-sectional aspect ratio of the failed slide, thereby thick landslides can act differently to thin landslides. As a landslide loses potential energy downslope, it requires a gain in energy to overcome its frontal ramp. Frey-Martinez et al. (2006) conclude that thicker landslides require more energy to ramp out on the seabed and tend to remain locked in their frontal confinement. Frontally emergent slides therefore are able to satisfy the energetic conditions required for them to move freely on the seafloor. The drop height (driving force) and depth of the basal shear surface (resisting force) have been demonstrated to be key controlling factors on confined or emergent emplacement styles in sub-lacustrine landslides (e.g Moernaut and De Batist 2011). More specifically, the drop height influences the gravitational potential energy and is the key driving force for the development of frontal emergence and the basal shear surface depth is the key restricting parameter. Hence the interaction between these two parameters largely determines if a landslide becomes emergent or remains confined. Moernaut and De Batist (2011) conclude that emergent landslides were characterized by gravitational potential energy that exceeded the potential energy required to ramp out of their stratigraphic position.

The along-strike changes in the basal shear surface and thus its toewall geometry mean we can hypotheses that the controls between the resisting and driving forces also vary. Considering these potential controls (i.e., slope angle, slide thickness, drop height) in light of the slide studied here, we note that the top of the slide varies from c. 1875 ms or 1814 m in its updip region to 3405 ms or 3289 m in the frontal margin, yielding a drop height of 1530 ms (1475 m) across strike. The depth of the basal shear surface and the slide thickness vary laterally, i.e., the basal shear surface is deepest to the SW (3600 ms or 3483 m ) and shallowest to the NE (3150 ms or 3047 m). Given that the driving forces is higher, accompanied by a thinner deposit, strong levels of emergence is demonstrated to the SE; conversely the slide is less emergent and approaches confinement where the slope is gentler, the slide thicker and the drop height smaller to the SW. Effectively the run-out becomes smaller and the stresses resulted in slightly increased compression as the deformation front tilted to the south west with the formation of thrust bound pop-up blocks.   The style of the shortening varies along strike and we have demonstrated in this study that the slide displays varying levels of frontal emergence and exhibits good development of pressure ridges (e.g. Prior et al. 1984).

Several stair-case like geometries are developed resulting in the formation of two or three frontal walls in the south, south-east and only one frontal ramp in the south west of the toe region.  The development of ramp and flat geometries in the basal shear surface of submarine landslides has been linked to variation in the geotechnical properties of the stratigraphy (e.g. Frey-Martinez et al. 2005; Solheim et al. 2005; Bull et al. 2009). Basal shear surfaces typically develop between formations with different shear strength and/or pore pressure regimes (e.g. Leynaud et al. 2007; Strasser et al. 2007). For example, formations with higher shear strength (resulting from lower pore pressures) enable the basal shear surface to step up to shallower stratigraphic levels. Along strike variations in lithology could, therefore, lead to along-strike changes in basal shear surface and toewall geometry. For example, the stair-case like geometry observed in the NE of the studied

slide may indicate that region was originally characterized by a more complex stratigraphy; i.e., two or more prominent weak layers with high pore pressure (i.e. the basal shear surface 'flats') were separated by stronger intervals.

## Lateral variability of intra-slide strain

This study demonstrates that the translating slide mass underwent strike-slip shearing, resulting in the formation of sinistral shear zones (Figs. 9 and 10c). Similar structures have been documented in Nugraha et al. (2019) and Steventon et al. (2019) where they are inferred to document shear zones and record strike-slip movement between flow cells. However, it is notable that this style of deformation occurred after bulk shortening of the slide mass against the toewall, after formation of the thrust-bound pop-ups. The origin of this two-phase, non-coaxial deformation style is not clear. Early shortening in the toe domain was likely associated with the expulsion of pore waters, and compaction and embrittlement of the evolving rock mass, ultimately, leading to the development of seismic-scale contraction structures. This process was spatially variable, possibly due to lateral changes in sediment porosity, pressure build-up, and the evolving rock strength, leading to the development of intra-slide flow cells and bounding shear zones, the former traveling downflow at speeds and/or at slightly different times. Our analysis and identification of the intra-slide structures shows the concentration of strain in specific areas of the slide.

Slope-parallel shears 'longitudinal' are linked to differences in slide transport speeds (Omeru and Cartwright, 2019; Bull et al. 2009; Gee et al. 2005; Masson et al. 1993). The development of these structures in this study suggests a complexity in the transportation speeds or a recording of different processes that are spaced out in time. Unlike the single-celled model (e.g Farrell 1984), several cells were active during the formation of the slide. In addition to this, several sub-orthogonal sets or 'slope-oblique' structures record internal shearing as transport speeds varied during slide emplacement. The sub-orthogonal shears may record transpression and provides evidence for strike/oblique slip component of deformation within the contractional domain.

Longitudinal shears separate Area A and B. These shears are narrow (c. 90 - 120 m-wide) and extends for c. 12 km, from an updip limit to the frontal toe region (see Fig. 13) and records internal variations of transport velocity within the slide. There is a slight change in the top surface relief between the two areas, with a vertical difference from c. 4 m to 6 m. Slope-oblique shears 'sub-orthogonal' separate area B from area C and is narrow (c. 60 – 90 m-wide) and extends for c. 21.5 km from an updip limit to the point where it merges with area C. The shears also support internal shearing connected to transport velocity variations with an oblique slip component of deformation to the bulk sediment transport direction. We observe a slight positive relief from area B to area C (8 m to 11 m).

Nugraha et al. (2019) infer that downslope-converging grooves suggest a convergent pathway of the Gorgon slide, due to clustering of megaclasts which slowed down the transport velocities and initiated the formation of longitudinal shears. With the missing observation of strong convergent grooves in our data, a possible explanation might be during emplacement of the slide, megaclasts are entrained from slope substrate into the deposit (Fig. 16 and 17). Volumetrically large quantities of the megaclasts in the frontal toe region might have slowed down the transport velocities of the

deposit in Area A compared to the surrounding material and initiated the longitudinal and sub-orthogonal shears, thus allowing areas B and C to travel further downdip. Another plausible explanation might be that in the vicinity of Area A, the slope material has a higher shear strength that slowed the ability of the slide to entrain more substrate effectively causing higher transport velocities in B and C and the development of shear zones through time.

Alsop and Marco (2014) demonstrated that first-order, single-cell MTD is comprised of several, second order flow cells that may interact locally during translation. This second order interaction is exemplified by our along-strike analysis of PB-10. The shear zones represent boundaries separating second-order flow cells. We are able to show how strain varied across-strike at a smaller scale, and the role this played in accommodating early shortening. For example, our analysis of thrusts and thrust bound pop-ups demonstrated that on a very local scale, intra-slide strain is relatively evenly distributed, being shared between kinematically linked structures.

## 8. Conclusions

We use a high-resolution 3D seismic reflection database to study in detail a Neogene slide identified within the deep-water passive margin, Angoche Basin, offshore Mozambique. The Submarine landslide is defined by an upslope (head), an intermediate (translational), and downslope (toe) zone. The upslope structure records the origin of the slide, but the downslope frontal toe margin provides new evidence of the sequence of forces that halted this huge submarine landslide. We extract several seismic attributes from seismic reflection data that allowed the identification of kinematic indicators such as lateral margins, megaclasts, longitudinal shears, sub-orthogonal shears and impressive fold-thrust belt systems. The characterization of the landslide enabled the gross transport direction to be identified.

We propose three potential emplacement scenarios. (1) a shear coupling where the overriding debris flow(s) transfers stress into the underlying and adjacent substrate till the shear stress of the flow exceeds the critical shear strength of the substrate thus allowing the entrainment of substrate material and the development of a deeper decollement level. (2) states that the slide and debrite are coeval, both propagating seawards along fracture surfaces developed along weak pre-existing surfaces. The slide creates a deformation front resulting from ploughing into basinal sediments and incorporates material ahead of it, forming impressive folds and thrusts. In scenarios 1 and 2, the slide and debrite are genetically related. (3) the slide was overprinted by a younger debrite, thus genetically *unrelated*. The emplacement of submarine slides with subsequent strain overprinting can often be difficult to prove with end member scenarios, a combination of several scenarios might be plausible in explaining the complex deformation history.

The development of a basal shear surface or zone is a fundamental process that develops along pre-existing planes of weakness. Our data allows us to analyze how the basal shear surface or zone developed. We propose a model by which the basal shear surface or zone incrementally propagates downdip and precedes significant deformation of the overlying slide mass, with material above this level being translated and possibly shortened before being incorporated into the main body of the evolving slide.

We show that the toe region underwent two distinct phases of deformation; (1) bulk shortening, parallel to the overall SE-directed emplacement direction, accommodated by the formation of NE-trending trending symmetric pop-up blocks bound by fore-thrusts and back-thrusts. Our analysis shows present and restored lengths of H1 of c.12 km and c.13 km, respectively, which equals contractional shear strains (as expressed and accommodated by seismically imaged thrusts) of c. 8%. This analysis shows that contraction formed resulting from horizontal translation of the slide over a short distance, c.8%. In addition, the interplay between driving forces and resisting forces determines the lateral variability of the frontal toe wall. In this study the submarine landslide is frontally emergent, with the driving forces largely exceeding resistive forces. We demonstrate that the geometry of the submarine landslide exhibits varying degrees of frontal emergence along strike, displaying a single frontal (toe) wall in the SW to a complex, stair-step geometry in the NE. We provide a detailed documentation of the along-strike variation in the structural style and evolution of the basal shear surface in the toe zone. A detailed study of a representative depth section within the region of the pop-up block showed the along-strike variability of the intra-slide strain. The cumulative throws show that strain broadly balances out although strain might be shared differently within flow cells. (2) the development of NW-trending sinistral shear zones that offsets the earlier formed shortening structures. The shear zones separate flow cells reflecting along-strike variations in the rate of downslope translation. These cells have previously been documented in the field at the cm- to m-scale, but with shortcomings on where or when they formed within the landslide. We have shown using 3D seismic reflection data how the shear zones relate to the overall kinematics of the submarine landslide, forming as a result of the translation of the deposit at varying internal velocities and/or at different times.

## Acknowledgements

## References

Alsop, G.I. and Marco, S. 2014. Fold and fabric relationships in temporally and spatially evolving slump systems: a multi-cell flow model. Journal of Structural Geology, 63, 27–49, https://doi.org/10.1016/j.jsg.2014.02.007

Alsop, G.I., Weinberger, R., Marco, S. and Levi, T. 2019. Fold and thrust systems in mass-transport deposits around the Dead Sea basin. American Geophysical Union, Geophysical Monograph Series, 246, 139–153, https://doi.org/10. 1002/9781119500513.ch9

Alves, T.M. 2015. Submarine slide blocks and associated soft-sediment deformation in deep-water basins: a review. Marine and Petroleum Geology, 67, 262–285, https://doi.org/10.1016/j.marpetgeo.2015.05.010

Alves, T.M. and Cartwright, J.A. 2009. Volume balance of a submarine landslide in the Espírito Santo Basin, offshore Brazil: quantifying seafloor erosion, sediment accumulation and depletion. Earth and Planetary Science Letters, 288, 572–580, https://doi.org/10.1016/j.epsl.2009.10.020

Alves, T.M., Kurtev, K., Moore, G.F. and Strasser, M. 2014. Assessing the internal character, reservoir potential, and seal competence of mass-transport deposits using seismic texture: a geophysical and petrophysical approach. AAPG Bulletin, 98, 793–824, https://doi.org/10.1306/09121313117

Bull, S. and Cartwright, J.A. 2019. Line length balancing to evaluate multi-phase submarine landslide development: an example from the Storegga Slide, Norway. Geological Society, London, Special Publications, 500, 531–549, https://doi.org/10.1144/SP500-2019-168

Bull, S., Cartwright, J. and Huuse, M. 2009. A review of kinematic indicators from mass-transport complexes using 3D seismic data. Marine and Petroleum Geology, 26, 1132–1151, https://doi.org/10.1016/j.marpetgeo.2008.09.011

Butler, R. and McCaffrey, W. 2010. Structural evolution and sediment entrainment in mass-transport complexes: outcrop studies from Italy. Journal of the Geological Society, London, 167, 617–631, https://doi.org/ 10.1144/0016-76492009-041

Cardona, S., Wood, L.J., Day-Stirrat, R.J. and Moscardelli, L. 2016. Fabric development and pore-throat reduction in a mass-transport deposit in the Jubilee Gas Field, Eastern Gulf of Mexico: consequences for the sealing capacity of MTDs. Advances in Natural and Technological Hazards Research, 41, 27–37, https://doi.org/10.1007/978-3-319-20979-1_3

Cardona, S., Wood, L.J., Dugan, B., Jobe, Z. and Strachan, L.J. 2020. Characterization of the Rapanui mass-transport deposit and the basal shear zone: Mount Messenger Formation, Taranaki Basin, New Zealand. Sedimentology, 67, 2111–2148, https://doi.org/10.1111/sed.12697

Dasgupta, P. 2008. Experimental decipherment of the soft sediment deformation observed in the upper part of the Talchir Formation (Lower Permian), Jharia Basin, India. Sedimentary Geology, 205, 100–110.

Dahlstrom, C. 1969. Balanced cross sections. Canadian Journal of Earth Sciences, 6, 743–757, https://doi.org/10.1139/e69-069

Dott, R. 1963. Dynamics of subaqueous gravity depositional processes. AAPG Bulletin, 47, 104–128.

Dunlap, D.B.,Wood, L.J., Weisebberger, C. and Jabour, H. 2010. Seismic geomorphology of offshore Morocco's east margin, Safi Haute Mer area. American Association of Petroleum Geologists Bulletin, 94, 615–642, https://doi.org/10.1016/j.marpetgeo.2008.09.011

Farrell, S.G. 1984. A dislocation model applied to slump structures, Ainsa Basin, South Central Pyrenees. Journal of Structural Geology, 6, 727–736, https:// doi.org/10.1016/0191-8141(84)90012-9

Francis, M., Milne, G., Kornpihl, D.K., Tewari, S., Rathee, D., Barlass, D. and Broadbent, K. 2017. Petroleum systems of the deepwater Mozambique Basin. First Break, 35(6) https://doi.org/2083/10.3997/1365-2397.35.6.89456

Frey-Martinez, J., Cartwright, J. and Hall, B. 2005. 3D seismic interpretation of slump complexes: examples from the continental margin of Israel. Basin Research, 17, 83–108, https://doi.org/10.1111/j.1365-2117.2005.00255.x

Frey-Martínez, J., Cartwright, J. and James, D. 2006. Frontally confined versus frontally emergent submarine landslides: a 3D seismic characterization. Marine and Petroleum Geology, 23, 585–604, https://doi.org/10.1016/j.marpetgeo.2006.04.002

Gee, M., Gawthorpe, R. and Friedmann, J. 2005. Giant striations at the base of a submarine landslide. Marine Geology, 214, 287–294, https://doi.org/10.1016/j.margeo.2004.09.003

Gee, M.J., Masson, D.G., Watts, A.B. and Mitchell, N.C. 2001. Passage of debris flows and turbidity currents through a topographic constriction: seafloor erosion and deflection of flow pathways. Sedimentology, 48, 1389–1409,https://doi.org/10.1046/j.1365-3091.2001.00427.x

Gee, M., Uy, H., Warren, J., Morley, C. and Lambiase, J. 2007. The Brunei slide: a giant submarine landslide on the North West Borneo margin revealed by 3D seismic data. Marine Geology, 246, 9–23, https://doi.org/10.1016/j.margeo.2007.07.009

Guntoro, A. 1999. The formation of the Makassar Strait and the separation between SE Kalimantan and SW Sulawesi. Journal of Asian Earth Sciences,17, 79–98, https://doi.org/10.1016/S0743-9547(98)00037-3

Hodgson,D., Brooks, H., Ortiz-Karpf, A., Spychala, Y., Lee, D. and Jackson, C.A-L.2018. Entrainment and abrasion of megaclasts during submarine landsliding and their impact on flow behaviour. Geological Society, London, Special Publications, 477, 223-240, https://doi.org/10.1144/SP477.26

Huvenne, V.A.I., Croker-Peter, F. and Henriet, J.P. 2002. A refreshing 3D view of an ancient sediment collapse and slope failure. Terra Nova, 14, 33–40, https://doi.org/10.1046/j.1365-3121.2002.00386.x

Jackson, C.A. 2011. Three-dimensional seismic analysis of megaclast deformation within a mass transport deposit; implications for debris flow kinematics. Geology, 39, 203–206, https://doi.org/10.1130/G31767.1

Leynaud, D., Sultan, N., Mienert, J., 2007. The role of sedimentation rate and permeability in the slope stability of the formerly glaciated Norwegian continental margin: the Storegga Slide model. Landslides 4 (4), 297–309.

Mahanjane, E.S. 2014. The Davie Fracture Zone and adjacent basins in the offshore Mozambique Margin: A new insight for the hydrocarbon potential Marine and Petroleum Geology, 57, 561-571. https://doi.org/10.1016/j.marpetgeo.2014.06.015

Mahanjane, E.S., and Franke, D., 2014. The Rovuma Delta deep-water fold-and-thrust belt, offshore Mozambique. Tectonophysics 614, 91-99. http://dx.doi.org/10.1016/j.tecto.2013.12.017.

Martel, S.J., 2004. Mechanics of landslide initiation as a shear fracture phenomenon. Marine Geology 203, 319–339.

Martinsen, O.J., 1989. Styles of soft-sediment deformation on a Namurian (Carboniferous) delta slope, western Irish Namurian Basin, Ireland. In: Whateley, M.K.G., Pickering, K.T. (Eds.), Deltas: Sites and Traps for Fossil Fuels. Geological Society of London Special Publication, vol. 210. pp. 167‑177.

Martinsen, O. and Bakken, B. 1990. Extensional and compressional zones in slumps and slides in the Namurian of County Clare, Ireland. Journal of the Geological Society, London, 147, 153–164, https://doi.org/10.1144/gsjgs.147. 1.0153

Masson, D., Huggett, Q. and Brunsden, D. 1993. The surface texture of the Saharan debris flow deposit and some speculations on submarine debris flow processes. Sedimentology, 40, 583–598, https://doi.org/10.1111/j.1365-3091. 1993.tb01351.x

McGilvery, T.A., Haddad, G. and Cook, D.L. 2004. Seafloor and shallow subsurface examples of mass transport complexes, Offshore Brunei. Onshore Technology Conference, Houston, TX.

Minisini, D., Trincardi, F., Asioli, A., Canu, M. and Foglini, F. 2007. Morphologic variability of exposed mass transport deposits on the eastern slope of Gela Basin (Sicily channel). Basin Research, 19, 217–240.

Moore, G.F., Saffer, D., Studer, M. and Pisani, P.C. 2011. Structural restoration of thrusts at the toe of the Nankai Trough accretionary prism off Shikoku Island, Japan: implications for dewatering processes.

Moernaut, J. and De Batist, M. 2011. Frontal emplacement and mobility of sub lacustrine landslides: Results from morphometric and seismostratigraphic analysis. Marine Geology 285, 29–45.

Moscardelli, L.,Wood, L. and Mann, P. 2006. Mass-transport complexes and associated processes in the Offshore Area of Trinidad and Venezuela. AAPG Bull., 90, 1059-1088.

Moscardelli, L. and Wood, L. 2008. New classification system for mass transport complexes in offshore Trinidad. Basin Research, 20, 73–98, https://doi.org/10.1111/j.1365-2117.2007.00340.x

Nardin, T.R., Hein, F., Gorsline, D.S. and Edwards, B. 1979. A review of mass movement processes sediment and acoustic characteristics, and contrasts in slope and base-of-slope systems versus canyon-fan-basin floor systems. SEPM Special Publications, 27, 61–74.

Nemec, W. 1991. Aspects of sediment movement on steep delta slopes. International Association of Sedimentologists, Special Publications, 10, 29–73.

Nugraha, H.D., Jackson, C.A.L., Johnson, H.D. and Hodgson, D.M. 2020. Lateral variability in strain along the toewall of a mass transport deposit; a case study from the Makassar Strait, offshore Indonesia. Geological Society of London, 177, 1261–1279. https://doi.org/10.1144/jgs2020-071

Ogata, K., Mutti, E., Pini, G.A. and Tinterri, R. 2012. Mass transport-related stratal disruption within sedimentary mélanges: examples from the northern Apennines (Italy) and south-central Pyrenees (Spain). Tectonophysics, 568, 185–199, https://doi.org/10.1016/j.tecto.2011.08.021

Ogata, K., Mountjoy, J., Pini, G.A., Festa, A. and Tinterri, R. 2014a. Shear zone liquefaction in mass transport deposit emplacement: a multi-scale integration of seismic reflection and outcrop data. Marine Geology, 356, 50–64, https://doi.org/10.1016/j.margeo.2014.05.001

Ogata, K., Pogacnik, Z, Pini, G.A., Tunis, G., Festa, A., Camerlenghi, A. and Rebesco, M. 2014b. The carbonate mass transport deposits of the Paleogene Friuli Basin (Italy/Slovenia): internal anatomy and inferred genetic processes. Marine Geology, 356, 88–110, https://doi.org/10.1016/j.margeo.2014.06.014

Ogata, K., Festa, A., Pini, G., Pogacnik, Z and Lucente, C. 2019. Substrate deformation and incorporation in sedimentary mélanges (olistostromes): examples from the northern Apennines (Italy) and northwestern Dinarides (Slovenia). Gondwana Research, 74, 101–125, https://doi.org/10.1016/j.gr.2019.03.001.

Olafiranye, K., Jackson, C.A.-L. and Hodgson, D.M. 2013. The role of tectonics and mass-transport complex emplacement on upper slope stratigraphic evolution: a 3D seismic case study from offshore Angola. Mar. Pet. Geol., 44, 196–216.

Omeru, T. and Cartwright, J.A. 2019. The efficacy of kinematic indicators in a complexly deformed mass transport deposit: insights from the deepwater Taranaki Basin, New Zealand. Marine and Petroleum Geology, 106, 74–87,https://doi.org/10.1016/j.marpetgeo.2019.04.037

Ortiz-Karpf, A., Hodgson, D.M. & Mccaffrey, W.D. 2015. The role of mass-transport complexes in controlling channel avulsion and the subsequent sediment dispersal patterns on an active margin: the Magdalena Fan, offshore Colombia. Marine and Petroleum Geology, 64, 58–75, https://doi.org/10.1016/j.marpetgeo. 2015.01.005

Ortiz-Karpf, A., Hodgson, D.M., Jackson, C.A.-L. and Mccaffrey, W.D. 2017. Influence of seabed morphology and substrate composition on mass-transport flow processes and pathways: insights from the Magdalena Fan, offshore Colombia. Journal of Sedimentary Research, 87, 189–209, https://doi.org/10.2110/jsr.2017.10

Ortiz-Karpf, A., Hodgson, D.M., Jackson, C.A.-L. and Mccaffrey, W.D. 2018. Mass-transport complexes as markers of deep-water fold-and-thrust belt evolution: insights from the southern Magdalena Fan, offshore Colombia. Basin Research, 30, 65–88, https://doi. org/10.1111/bre.12208

Pedersen, S.I., Randen, T., Sønneland, L. and Steen, Ø. 2002. Automatic fault extraction using artificial ants. SEG Annual Meeting. (Conference Paper)

Posamentier, H.W. and Kolla, V. 2003. Seismic geomorphology and stratigraphy of depositional elements in deep-water settings. Journal of Sedimentary Research, 73, 367–388, https://doi.org/10.1306/111302730367

Posamentier, H.W. and Martinsen, O.J. 2011. The character and genesis of submarine mass-transport deposits: insights from outcrop and 3D seismic data. SEPM, Special Publications, 96, 7–38, https://doi.org/10.2110/sepmsp.096.007.

Prior, D.B., Bornhold, B.D. and Johns, M.W. 1984. Depositional characteristics of a submarine debris flow. Journal of Geology, 92, 707–727, https://doi.org/10.1086/ 628907

Ramsey, J.C. and Lisle, R.J. 2000. The Techniques of Modern Structural Geology. Academic Press, London.

Reeves, C. and Mahanjane, E.S., 2013. Mozambique and its role in the downfall of Gondwana. Geological Society of Houston/Petroleum Exploration Society of Great Britain, London, 2013 September 11-12. http://pesgb.org.uk/events/event-165/.

Reis, A.T., Araújob, E. 2016. Effects of a regional décollement level for gravity tectonics on late Neogene to recent large-scale slope instabilities in the Foz do Amazonas Basin, Brazil. Marine and Petroleum Geology, 75, 29–52, https://doi.org/10.1016/j.marpetgeo. 2016.04.011

Salman, G. and Abdula, I., 1995. Development of the Mozambique and Ruvuma sedimentary basins, offshore Mozambique. Sedimentary Geology 96, 7-41. Elsevier Science B.V. SSDI 0037-0738(94)00125-1.

Sammartini, M., Moernaut, J., Kopf, et al., Propagation of frontally confined subaqueous landslides: Insights from combining geophysical, sedimentological, and geotechnical analysis, *Sedimentary Geology* (2021), https://doi.org/10.1016/j.sedgeo.2021.105877

Sapri, D.H., Mahmud, O.T. and Wong Wi Chenm, H. 2013. Sequence Stratigraphic Study of Areas 3 & 6, Rovuma Basin Mozambique. *International Petroleum Technology Conference IPTC,* Extended Abstracts.

Scarselli, N., Mcclay, K. & Elders, C. 2013. Submarine Slide and Slump Complexes, Exmouth Plateau, NW Shelf of Australia. In: Western Australian Basins Symposium 2013, Aug 18–21 2013 Perth (Ed. by M. Keep & S.J. Moss). Petroleum Exploration Society of Australia.

Schnellmann, M., Anselmetti, F.S., Giardini, D. and McKenzie, J.A. 2005. Mass movement-induced fold-and-thrust belt structures in unconsolidated sediments in Lake Lucerne (Switzerland). Sedimentology, 52, 271–289, https://doi.org/10.1111/j.1365-3091.2004.00694.x

Sobiesiak, M.S., Kneller, B., Alsop, G.I. and Milana, J.P. 2018. Styles of basal interaction beneath mass transport deposits. Marine and Petroleum Geology, 98, 629–639, https://doi.org/10.1016/j.marpetgeo.2018.08.028

Sobiesiak, M.S., Buso, V.V., Kneller, B., Alsop, G.I. and Milana, J.P. 2019. Block generation, deformation, and interaction of mass-transport deposits with the seafloor: an outcrop-based study

of the Carboniferous Paganzo Basin (Cerro Bola, NW Argentina). American Geophysical Union, Geophysical Monograph Series, 246, 91–104, https://doi.org/10.1002/9781119500513.ch6

Solheim, A., Berg, K., Forsberg, C.F., Bryn, P., 2005. The Storegga Slide: repetitive large scale sliding with similar cause and development. Marine and Petroleum Geology 22, 97–107.

Steventon, M.J., Jackson, C.A., Hodgson, D.M. and Johnson, H.D. 2019. Strain analysis of a seismically imaged mass-transport complex, offshore Uruguay. Basin Research, 31, 600–620, https://doi.org/10.1111/bre.12337

Strasser, M., Anselmetti, F.S., Fah, D., Giardini, D., Schnellmann, M., 2006. Magnitudes and source areas of large prehistoric northern Alpine earthquakes revealed by slope failures in lakes. Geology 34 (12), 1005–1008.

Strasser, M., Stegmann, S., Bussmann, F., Anselmetti, F.S., Rick, B., Kopf, A., 2007. Quantifying subaqueous slope stability during seismic shaking: Lake Lucerne as model for ocean margins. Marine Geology 240 (1–4), 77–97.

Suppe, J. and Medwedeff, D.A. 1990. Geometry and Kinematics of Fault Propagation Folding. Eclogae Geologicae Helvetiae, 83, 409-454.

Totake, Y., Butler, R.W., Bond, C.E. and Aziz, A. 2018. Analyzing structural variations along strike in a deep-water thrust belt. Journal of Structural Geology, 108, 213–229, https://doi.org/10.1016/j.jsg.2017.06.007

Trincardi, F. and Argnani, A. 1990. Gela submarine slide: a major basin-wide event in the Plio-Quaternary foredeep of Sicily. Geo-Mar. Lett., 10, 13–21.

Van der Merwe, W., Hodgson, D., & Flint, S. 2009. Widespread syn-sedimentary deformation on a muddy deep-water basin-floor: The Vischkuil Formation (Permian), Karoo Basin, South Africa. *Basin Research* , *21* , 389 – 406 . https://doi.org/10.1111/j.1365-2117. 2009.00396.x

Van Der Merwe, W.C., Hodgson, D.M. and Flint, S.S. 2011. Origin and terminal architecture of a submarine slide: a case study from the Permian Vischkuil Formation, Karoo Basin, South Africa. Sedimentology, 58, 2012–2038, https://doi.org/10.1111/j.1365-3091.2011.01249.x

Van Bemmel , P. P. , & Pepper , R. E. 2000. *Seismic signal processing method and apparatus for generating a cube of variance values.* Google Patents.

Watt, S., Talling, P., et al. 2012. Widespread and progressive seafloor-sediment failure following volcanic debris avalanche emplacement: landslide dynamics and timing offshore Montserrat, Lesser Antilles. Marine Geology, 323, 69–94, https://doi.org/10.1016/j.margeo.2012.08.002

Weimer, P. 1990. Sequence stratigraphy, facies geometries, and depositional history of the Mississippi Fan, Gulf of Mexico (1) . *AAPG Bulletin* , *74* , 425 – 453.

Weimer, P. and Shipp, C. 2004. Mass transport complexes: musing on past uses and suggestions for future directions. Offshore Technology Conference, 3–6 May 2004, Houston, TX, USA, https://doi.org/10.4043/16752-MS

Wu, N., Jackson, CA., Johnson, H.D., Hodgson, D.M. and Nugraha, H.D. 2020. Mass-transport complexes (MTCs) document subsidence patterns in a northern Gulf of Mexico salt minibasin. Basin Research, 32, 1300-1327, https://doi.org/10.1111/bre.12429

Wu, N., Jackson, CA-L., Johnson, H.D., Hodgson, D.M., Clare, M.A., and Nugraha, H.D. 2020. The formation and implications of giant blocks and fluid escape structures in submarine lateral spreads. Basin Research. ISSN 0950-091X (In Press)

Zeng, H., Henry, S.C. and Riola, J.P. 1998. Stratal slicing, Part II: real 3-D seismic data. Geophysics, 63, 514–522, https://doi.org/10.1190/1.1444352

**Figure captions**

**Figure 1.** Location of the study area and bathymetric map of the Angoche Basin, offshore Mozambique (Sandwell and Smith 2000). An outline of the 3D time seismic surveys is represented by red rectangles and the 3D depth seismic by black rectangle. Drilled wells are represented by black filled circles and field outlines in red. Key river systems and lakes are also highlighted. Bathymetric contours are shown by the black lines in 500m increments.

**Figure 2.** (A) Dip seismic section, (B) geoseismic section, through the central part of the 3D broadband time-migrated seismic reflection data that covers c. 15,041 km$^2$. Chaotic packages, representing submarine landslides, are prominent throughout the Neogene interval.

**Figure 3.** Stratigraphic chart constructed based on regional correlation and seismic interpretation (modified from Mahanjane 2014)

**Figure 4.** (A) Dip seismic section illustrating structural geometries developed in the toe region. The slide is bound by a basal-shear surface (orange) at the base and a top surface (blue) at the top. The basal shear surface cuts up through stratigraphy to define the slides lateral margins. A steep frontal ramp (c. 210m.) defines the downdip limit of the toe region. (B-C) Strike seismic sections highlighting the geometry and scale of the slide lateral margins. The basal-shear surface shows discontinuities in the form of ramps that locally discordant to underlying stratigraphy.

**Figure 5.** (A) Thickness map of the slide between the basal-shear surface and the top surface illustrating significant thickening in the toe region. (B) a map-view of the variance attribute extracted from the basal shear surface (see Fig. 4). Several kinematic indicators are observable, including the slide lateral margins.

**Figure 6.** (A) Thickness map of the slide between the basal-shear surface and the top surface within the toe region. For location see Fig. 5A. (B) a map-view of the RGB attribute extracted from an isoproportional slice halfway between the top surface and the basal shear surface in the toe region; this highlights the key structural features within the slide body. The inner fold-and-thrust-belt is comprised of pop-up structures, whereas the outer fold-and-thrust-belt is dominated by pressure ridges.

**Figure 7.** Seismic facies classification used in this study. (A) Seismic facies description and interpretation (Table 1). (B) RGB attribute extraction from an iso-proportional slice (midway between the basal shear surface and the top surface). (C-E) Vertical sections showing seismic facies SF1 – SF3 within the slide.

**Figure 8.** (A) Dip illumination map of the basal shear surface in the slide toe region, delineating the lateral margins. (B) Interpretation of the basal shear surface showing the location of the grooves around the toe region of the slide.

**Figure 9.** Toe region of the slide. (A) Variance slice within the internal body of the slide, uninterpreted, note locations of figures 11 and 12. (B) Interpreted map highlighting lateral margins, fold-and-thrust structures and illustrating the internal interaction between slope-parallel shears 'longitudinal' and slope-oblique shears 'sub-orthogonal' within the toe region of the slide.

**Figure 10.** (A) Perspective 3D view of the subsurface elevation of the basal shear surface of the slide within the toe region of the slide highlighting the strike variability in the frontal ramp geometry. (B) Amplitude contrast extraction using a proportional slice between the basal shear surface and the top surface that illustrates key kinematic indicators including impressive thrust structures and pop-up blocks, uninterpreted. (C) Interpreted 3D view using a proportional slice between the basal shear surface and the top surface that illustrates key kinematic indicators, including thrust structures and pop-up blocks and shear zones within the toe region.

**Figure 11.** Interpreted seismic section showing well developed pop-up structures in the toe region and one major frontal wall in the SW part of the slide.

**Figure 12.** Interpreted seismic section showing pop-up structures in the toe region and a stair-step geometry in the north-eastern part of the slide.

**Figure 13.** 3D distribution of key kinematic features and the relationships between intra-slide structures. The display highlights the entrainment of megaclasts within the internal body of the deposit and the relative positions of the shear zones that separate flow cells reflecting along-strike variations in the rate of downslope translation.

**Figure 14.** Quantitative analysis of shortening strains associated with a thrust-bound pop-up block in the submarine landslide toe domain. (A) Depth-structure map of H1 and associated faults. (B) Variance extracted on H1 showing the lateral extent of pop-up block 10. Two shear zones separate the flow cells that have varying amounts of strain. Sinistral offsets are evident across the shear zone in the SW; more subtle offsets are seen to the NE. (C) Throw v. distance $(T - x)$ plot of fore- and back-thrusts bounding pop-up block 10. There is no major change in throw across the shear zones.

**Figure 15.** (A-C) Seismic sections showing the along strike variability of the faults bounding pop-up block 10

**Figure 16.** (A) Dip seismic sections illustrating contractional structures forming ahead of the flow and entrainment of large fragments from seabed as the debrite flowed. (B-C) Dip seismic sections highlights progressive imbrication downslope and the formation of regularly spaced pop-up blocks bounded by thrust planes. The basal shear surface or zone incrementally propagates downdip *ahead* of the developing slide mass  (D) Vertical seismic section illustrates the material above the basal shear surface is fully incorporated into the main body of the slide.

**Figure 17.** (A-B) illustrates the distributed shear zone formed ahead of the slides frontal toe wall. Note location of this figure in relation to larger slide in figure 16.

**Figure 18.** (A-B) Emplacement model describing the slide and debrite as being genetically related, scenario 2. Slope failure and slide triggering occur due to pore pressure build-up along a discrete layer or closely spaced layers and reduced shear strength of interval.  The slide ploughs and incorporates material ahead of it, forming folds and thrusts.  Note that the shear fracture deformation at depth precedes large displacements in the slide mass. (C) Impressive contractional structures formed in the region. (D-F)Vertical seismic sections showing relationship between overlying debrite and thrust bound pop-up blocks in the toe region.

**Table 1**

Description and interpretation of submarine landslide seismic facies used in this study.

**Appendix 1**

Selected seismic attributes used to reveal internal and external geometry of the slide in this study.
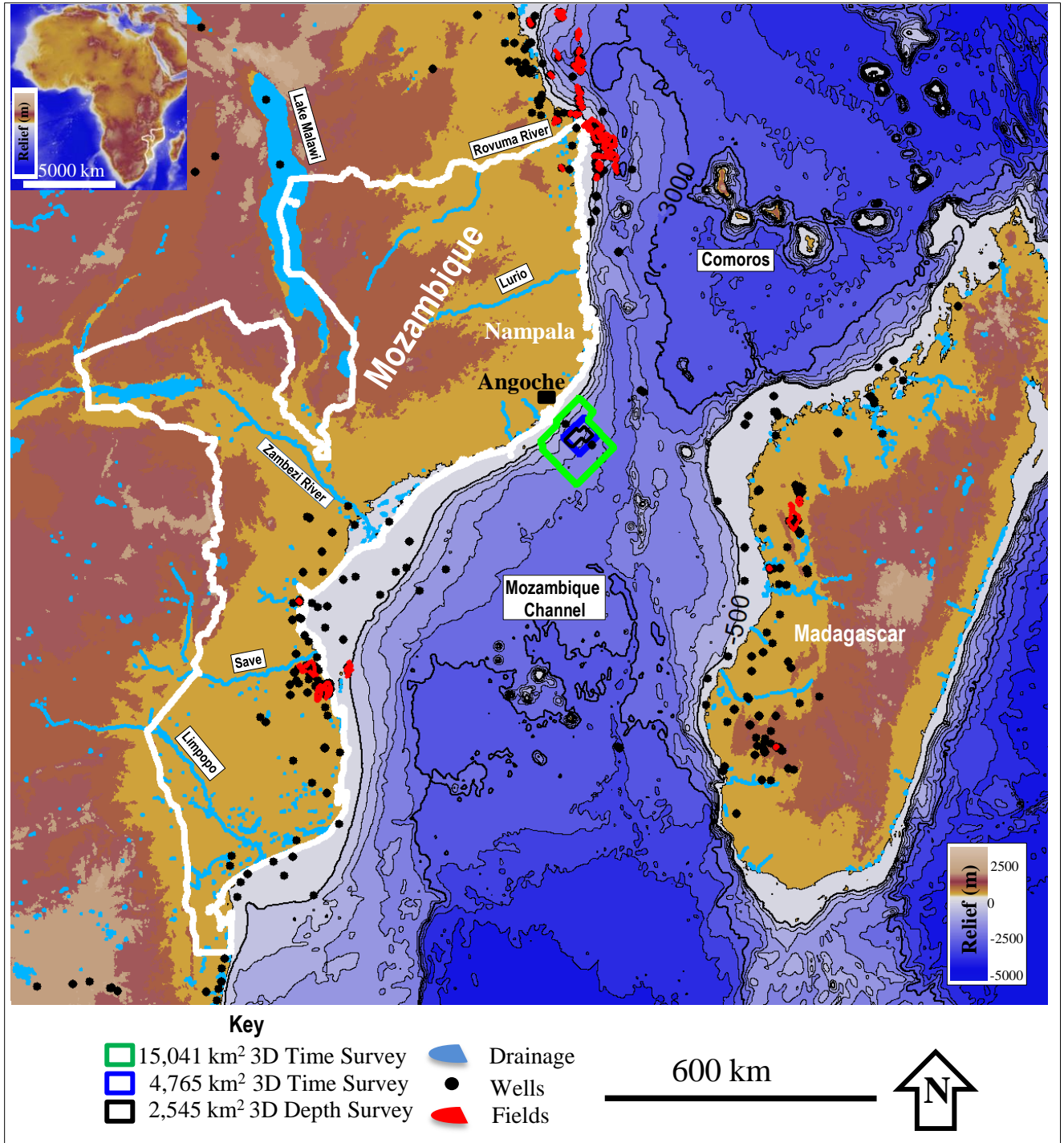
Figure 1
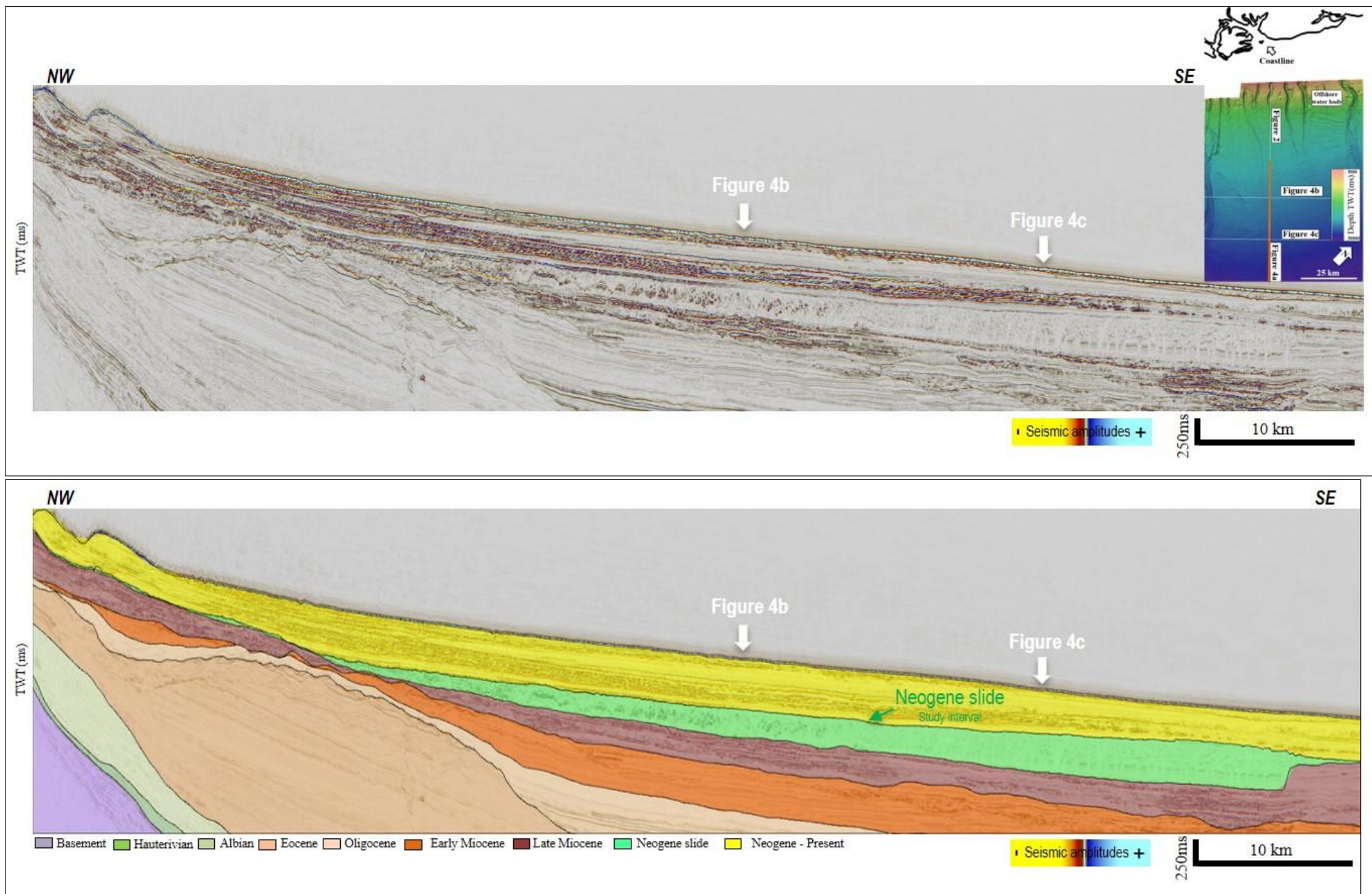
Figure 2
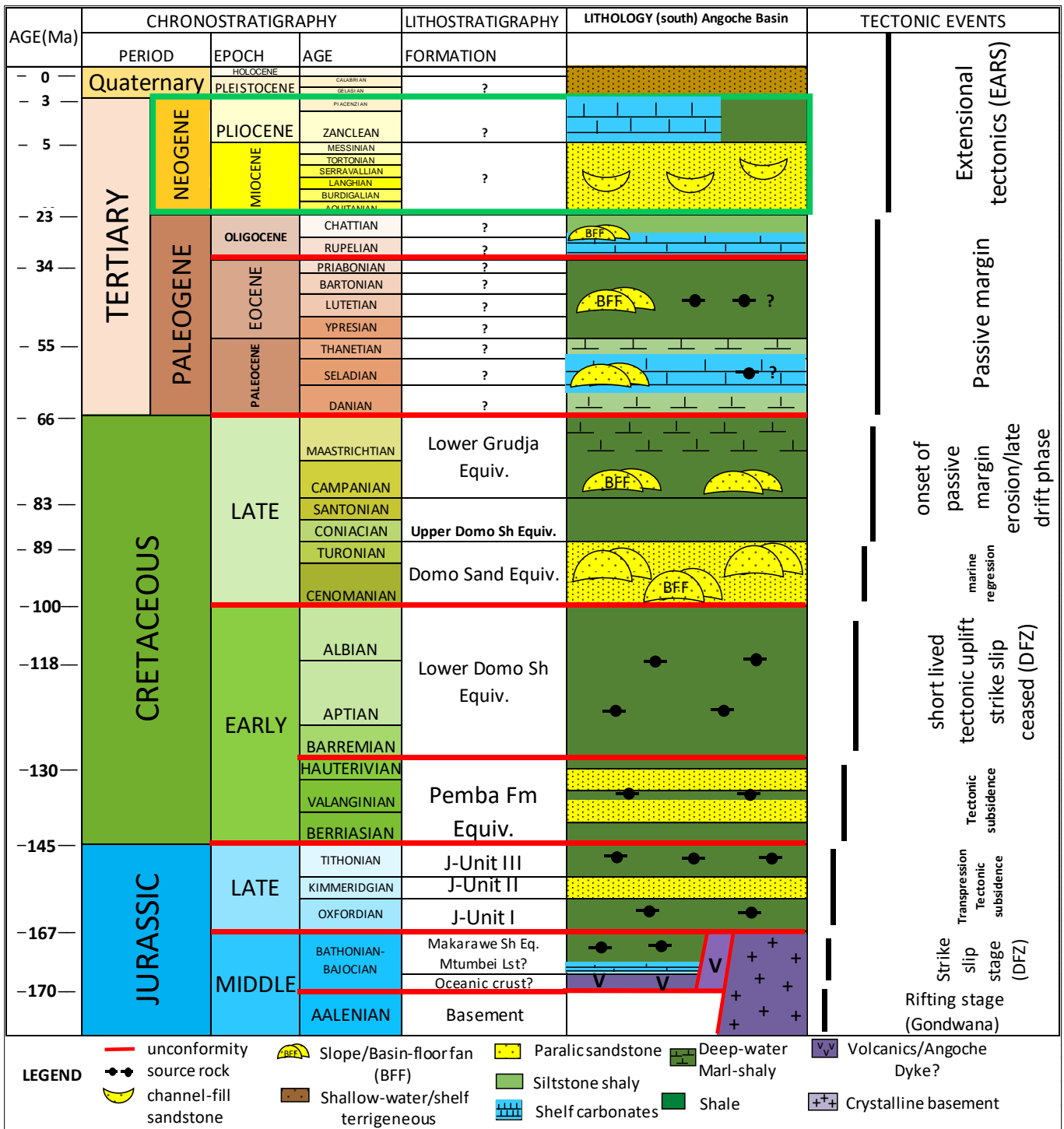
Figure 3

Figure 4

Figure 5

(A) Thickness Map

(B) Isoproportional slice

Thickness (ms)

400

0

10 km

N

Inner fold-and-thrust belt

Outer fold-and-thrust belt

10 km

N
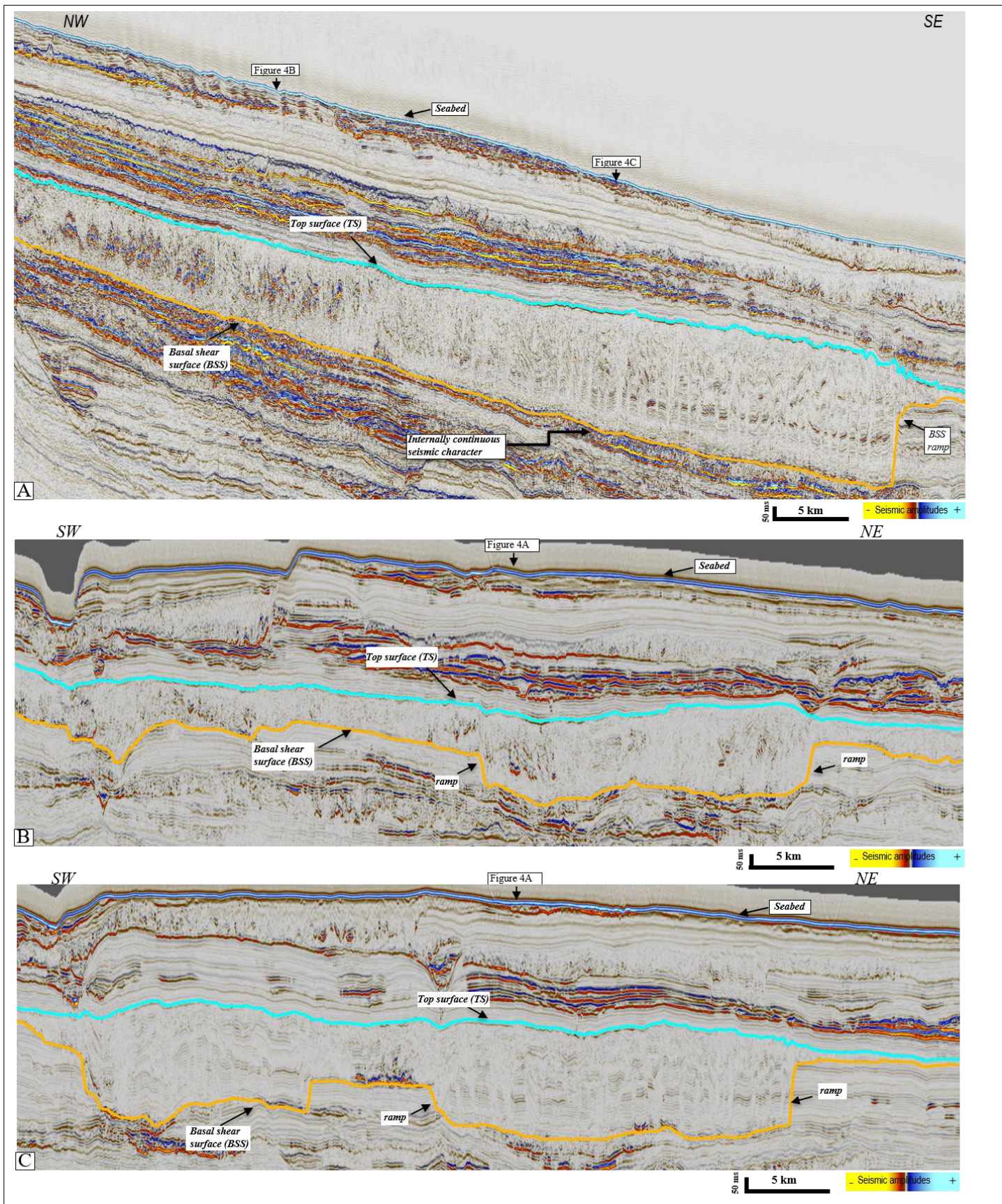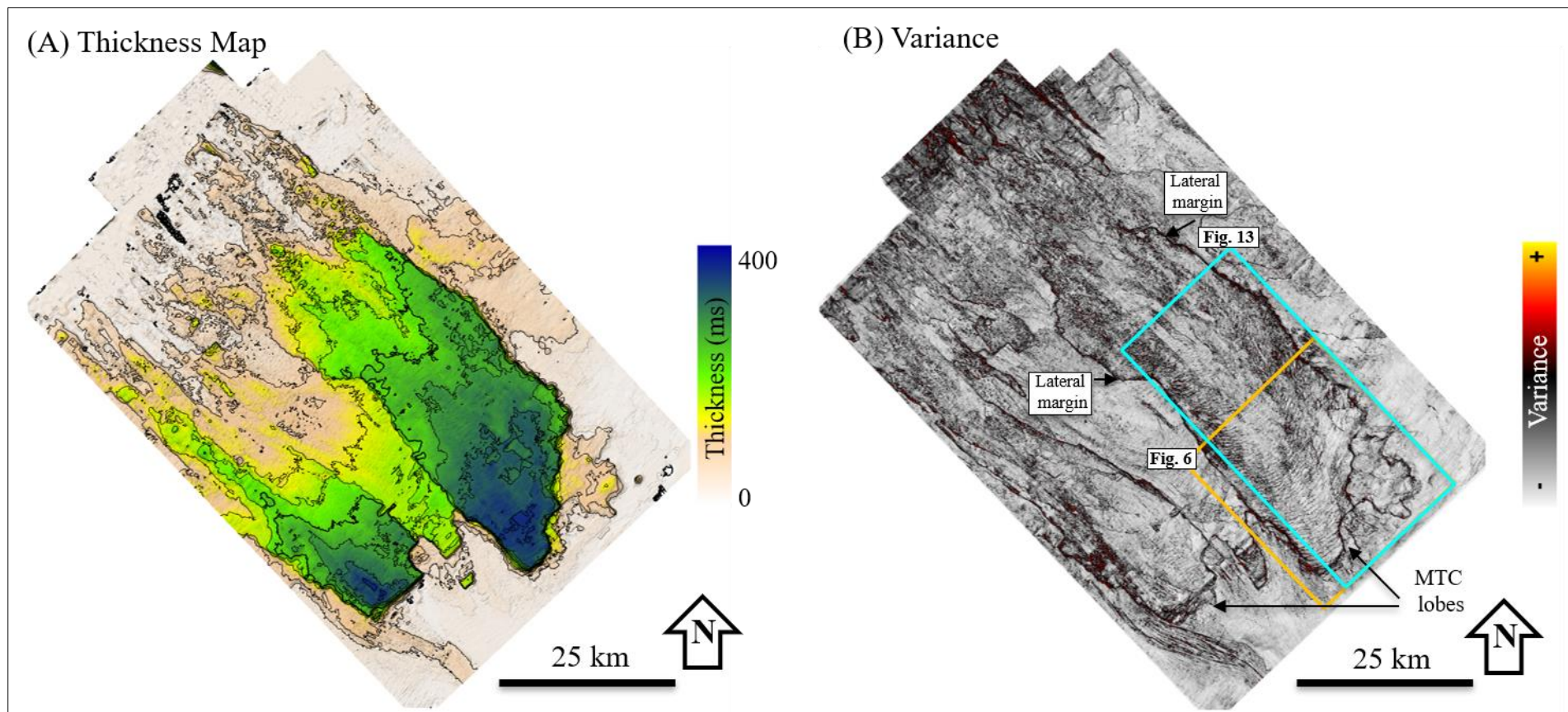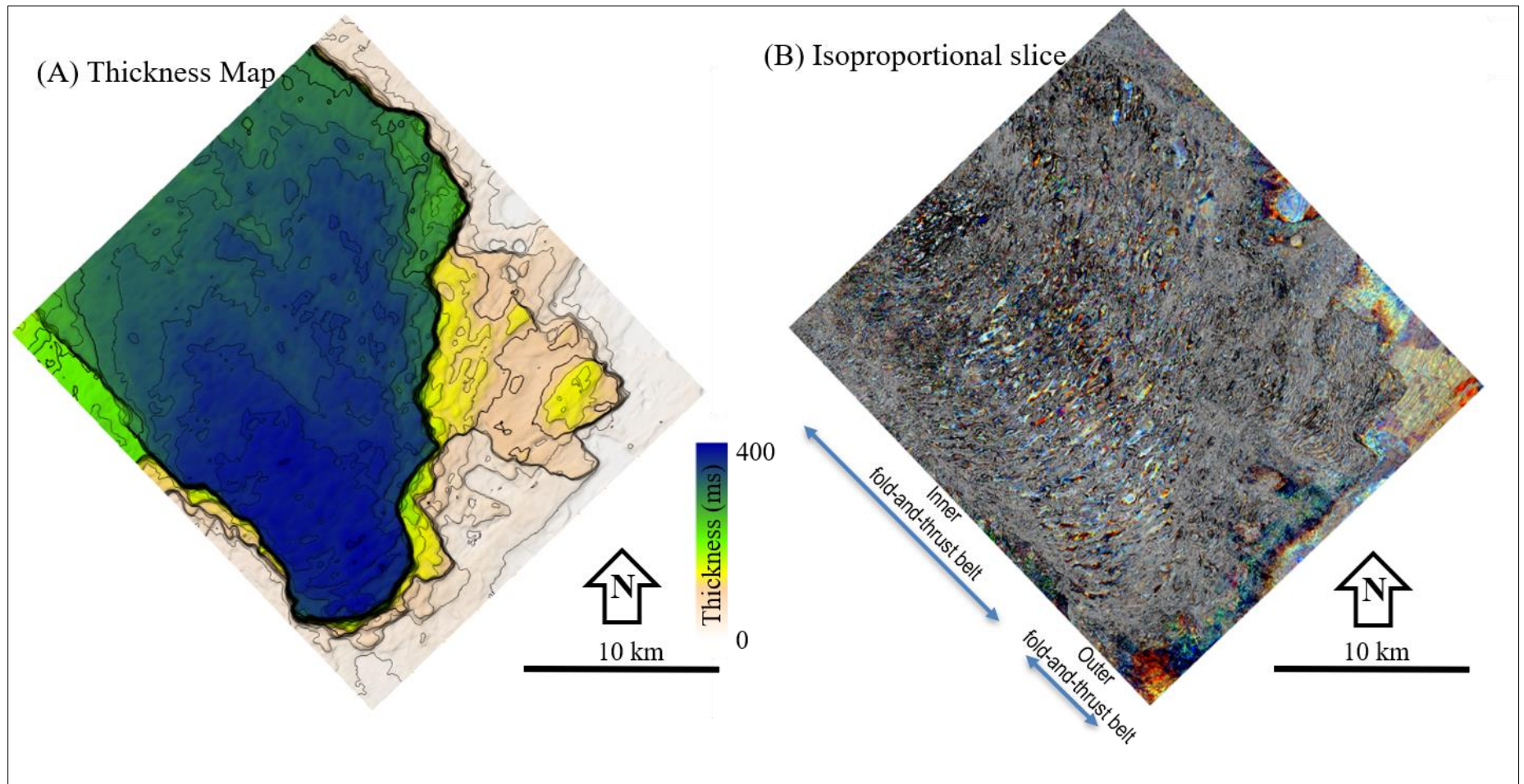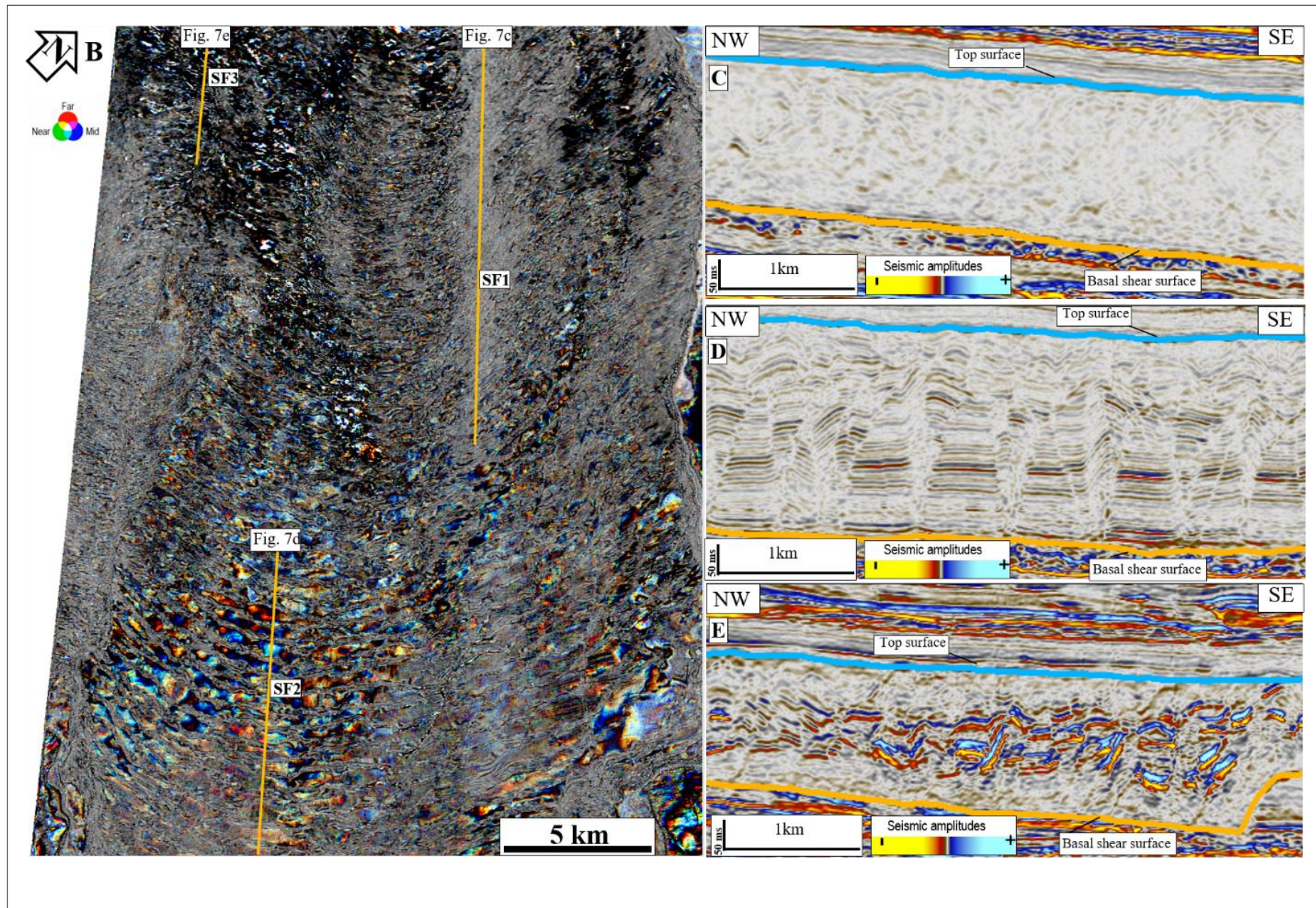
Figure 6

Figure 7

Figure 8

Figure 9

A

Depth

TWT (ms)

- 3150

- 3600

Frontal
ramp

Strike variability in
frontal ramp
geometry

2 km

N

B

Amplitude contrast

0.6

0.1

N

2 km

C

Lateral margin

Pressure ridges

Shear zones

Fold and thrust systems

Basal shear surface

Frontal ramp

Strike variability in frontal ramp geometry

N

2 km
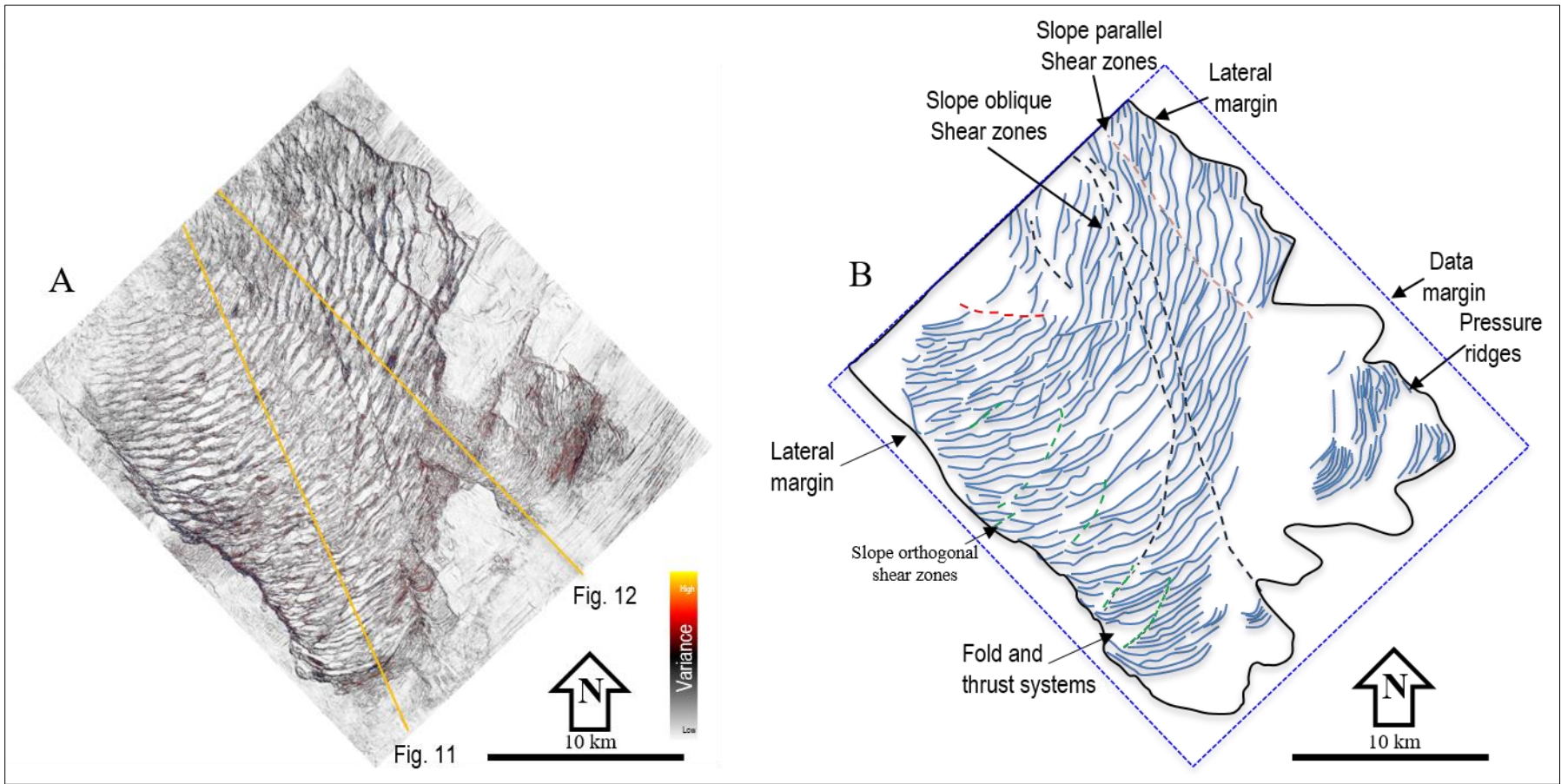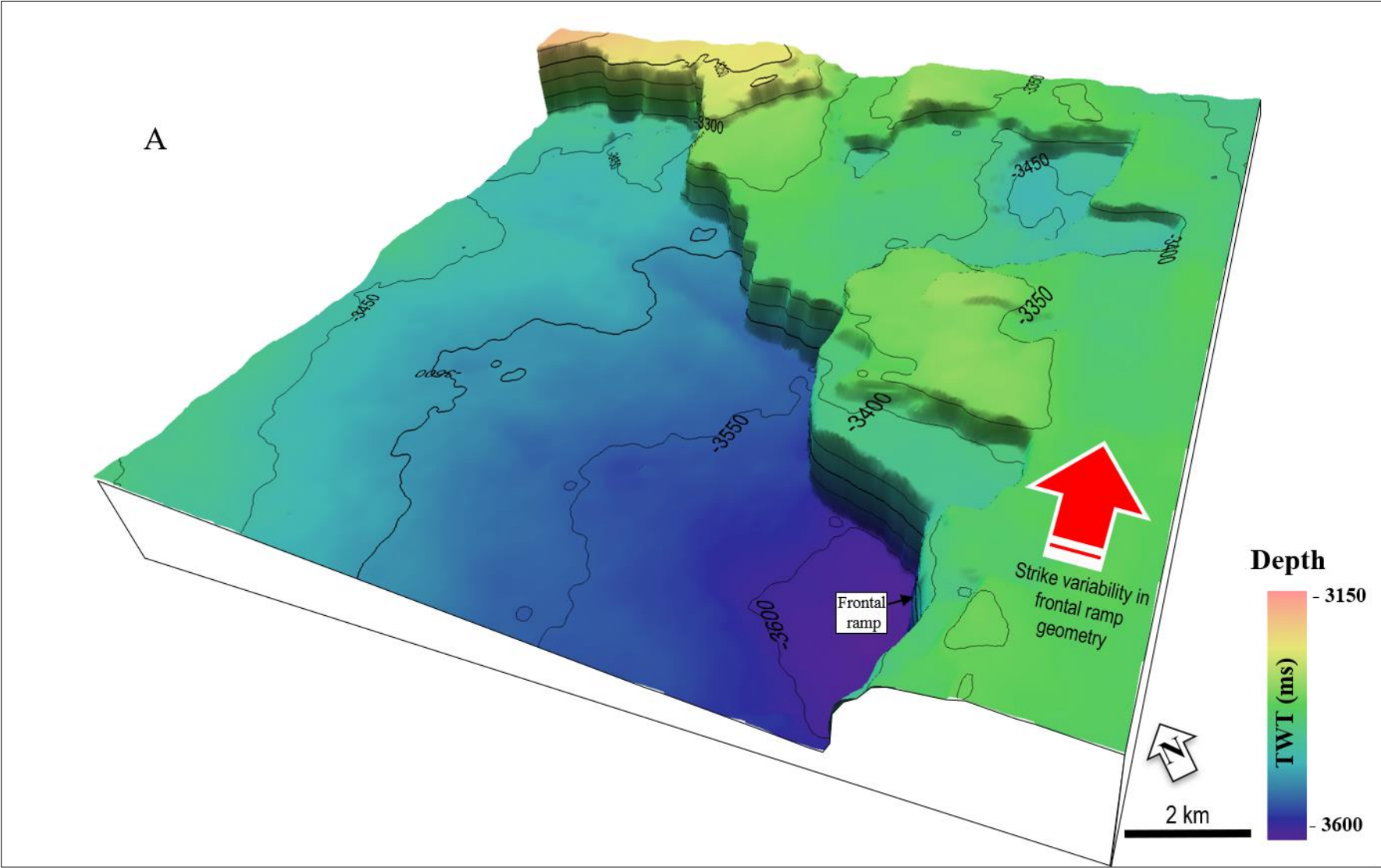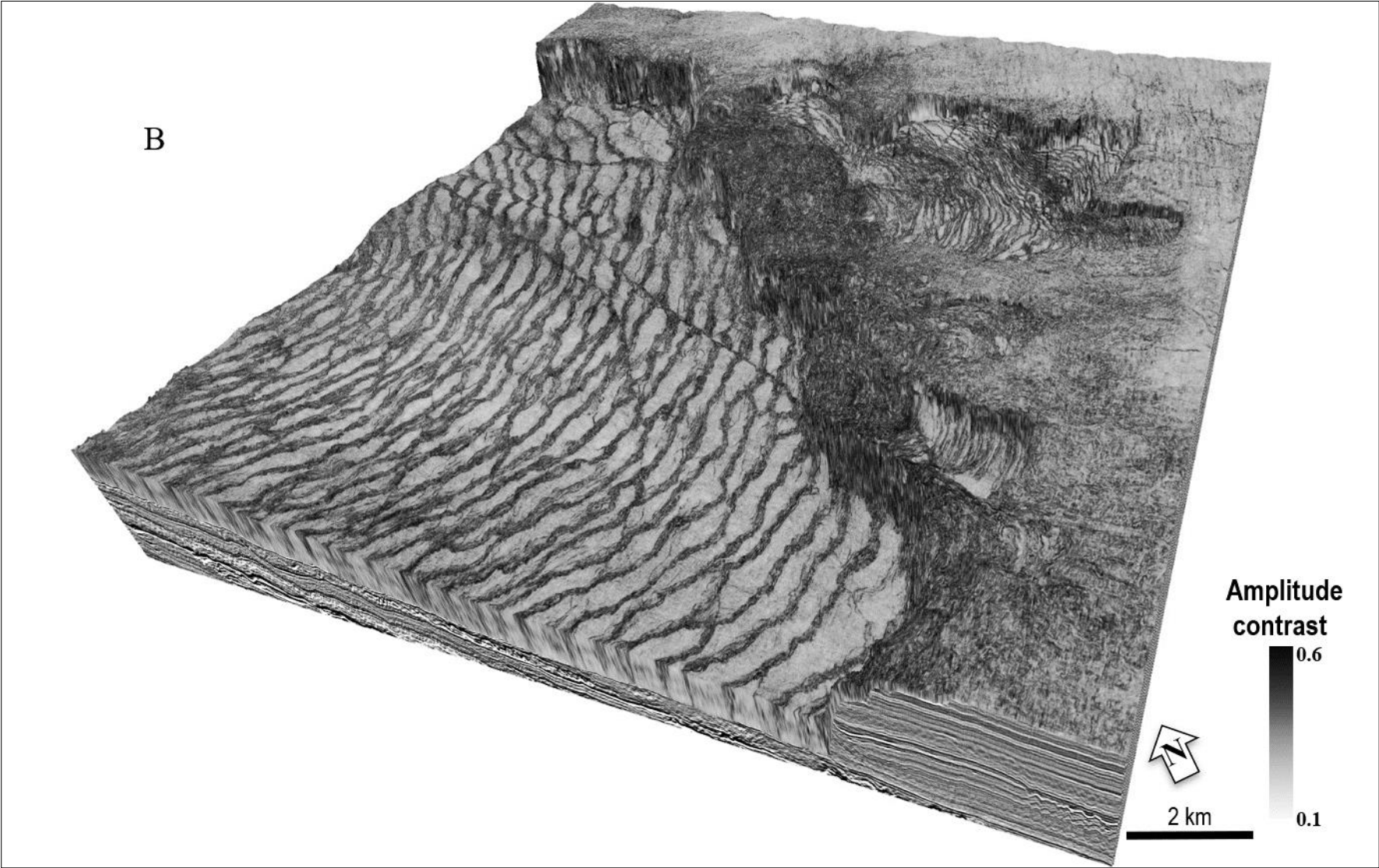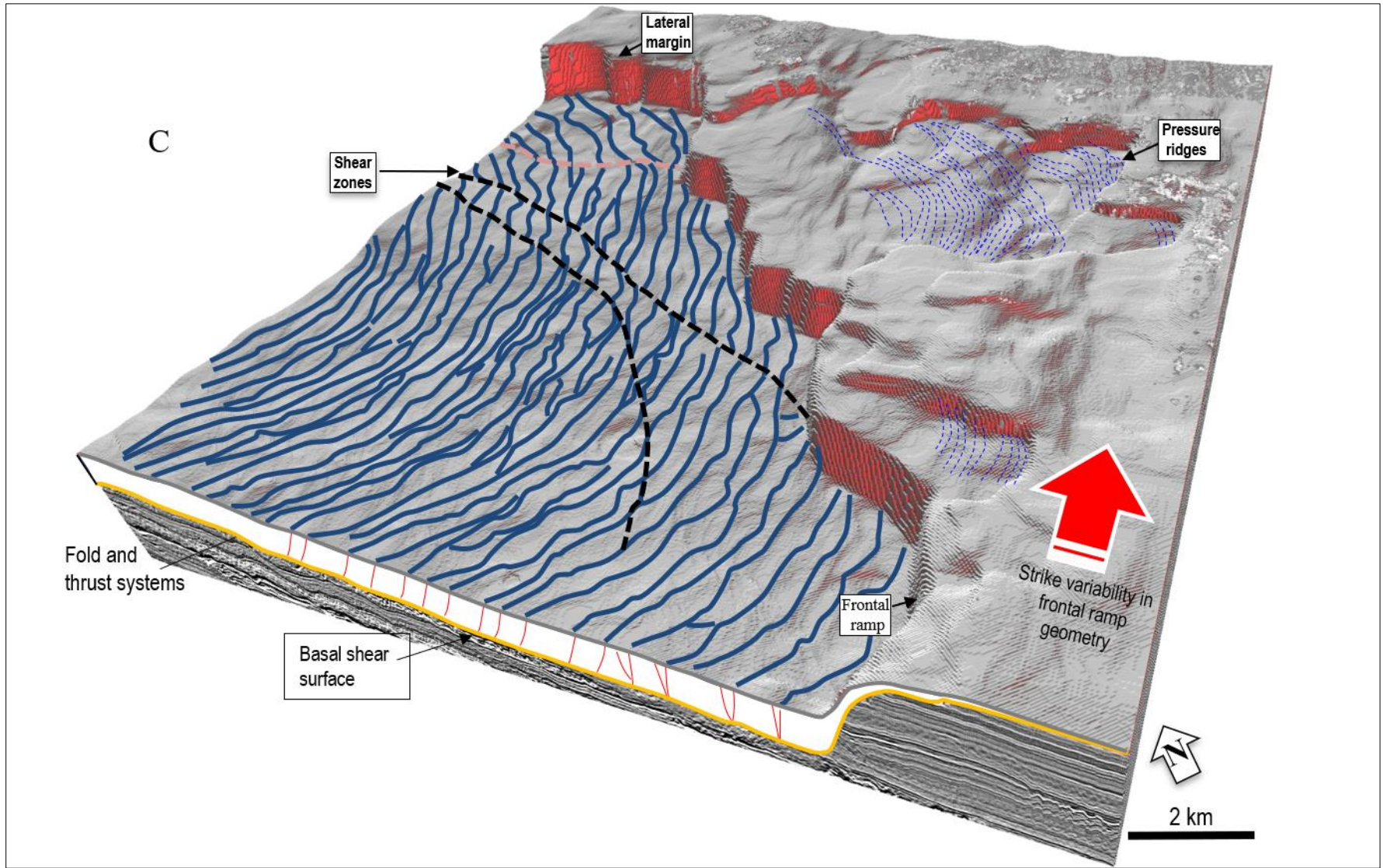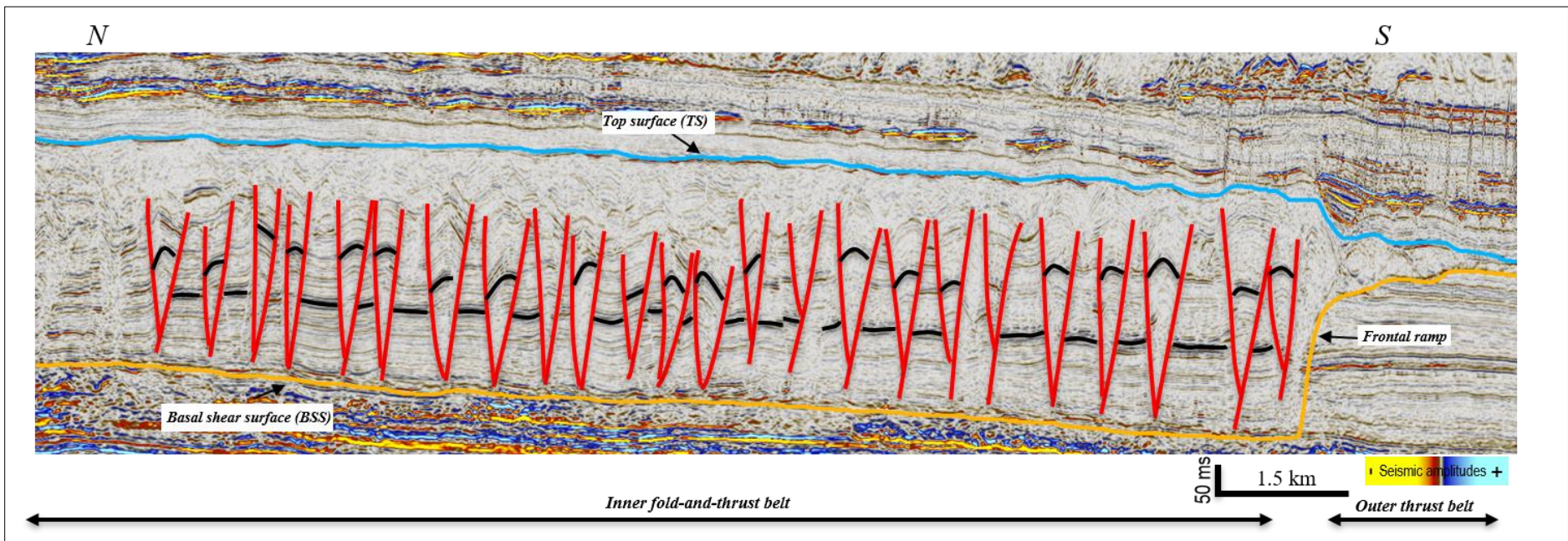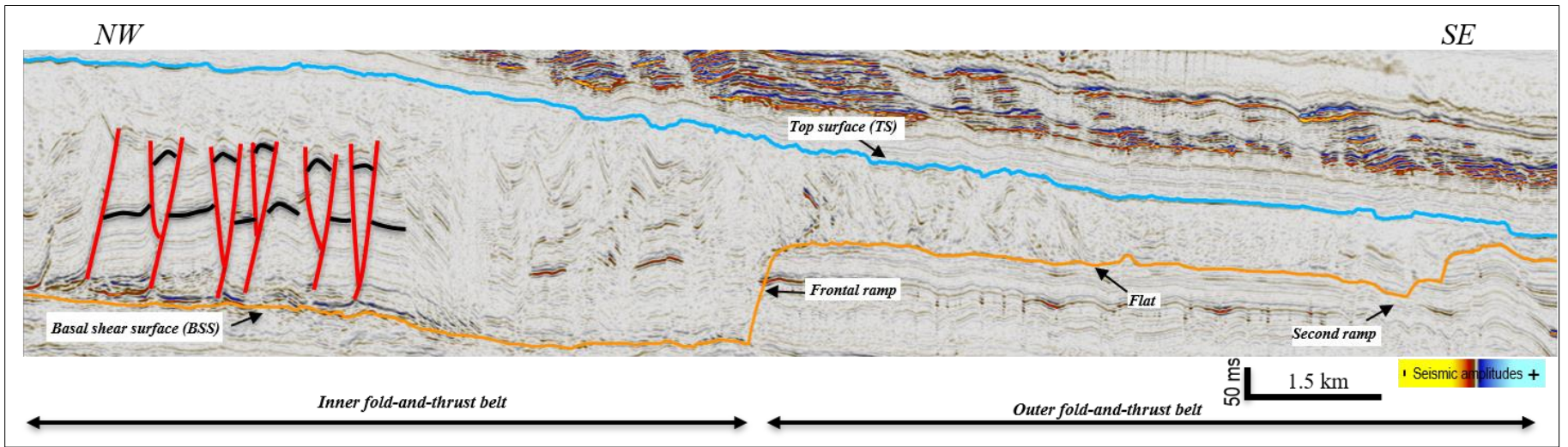
Figure 10

Figure 11

Figure 12

Figure 13

A
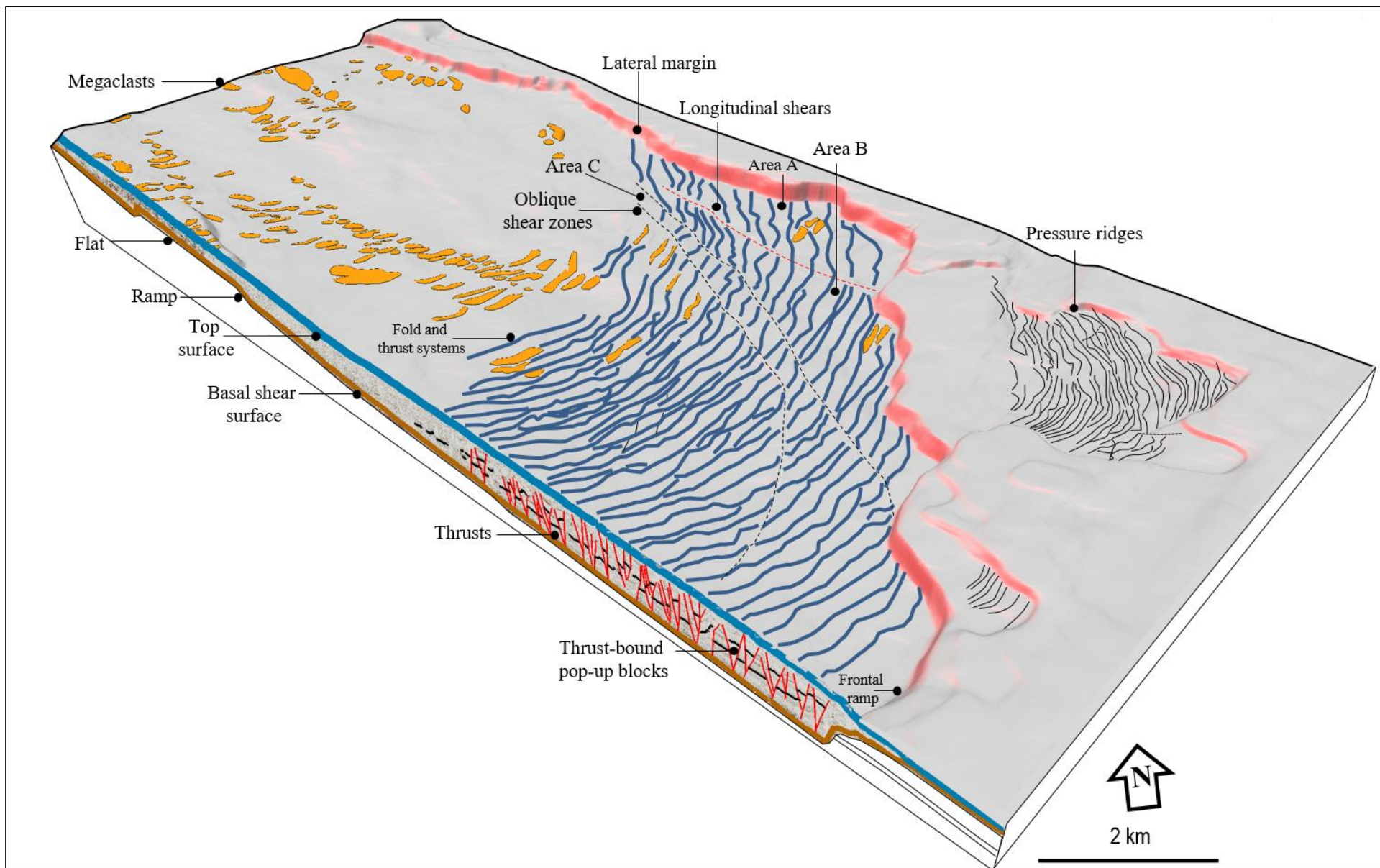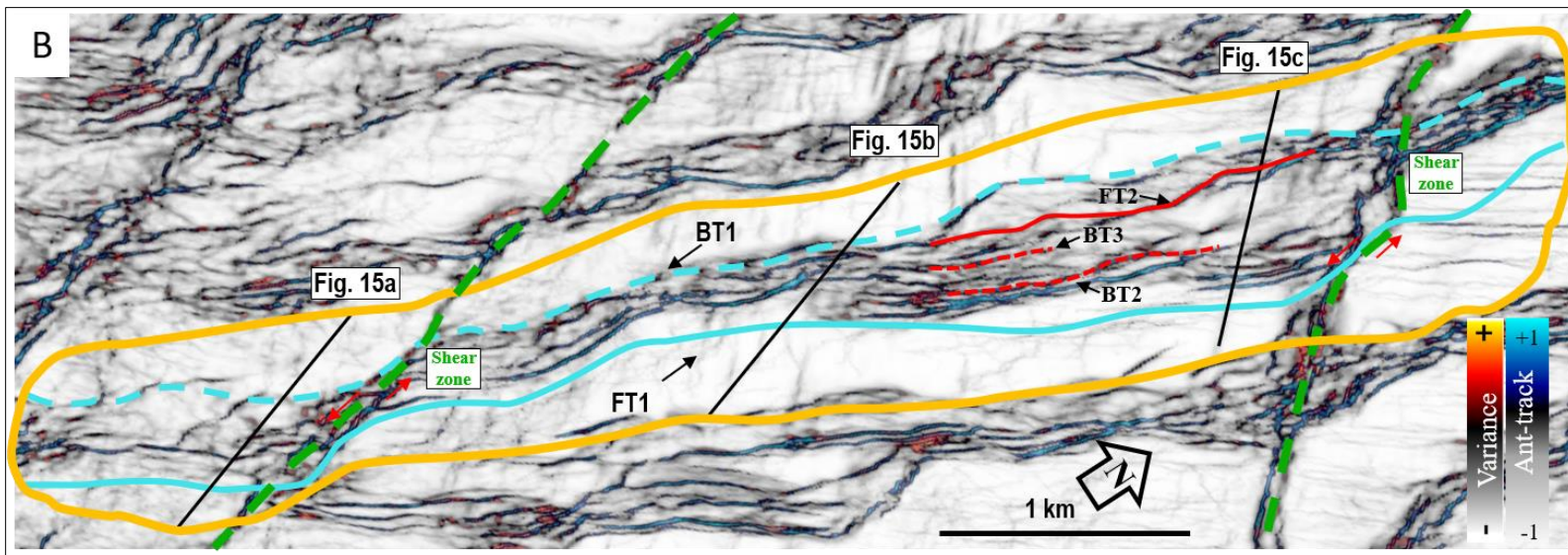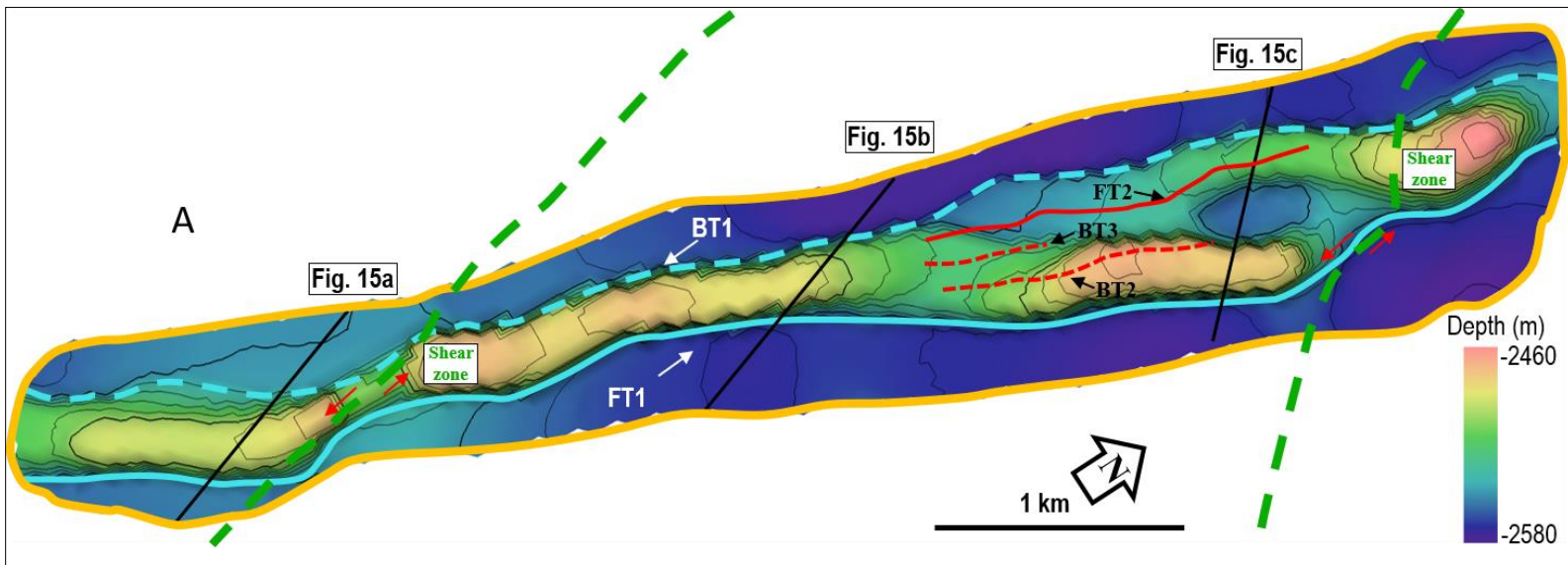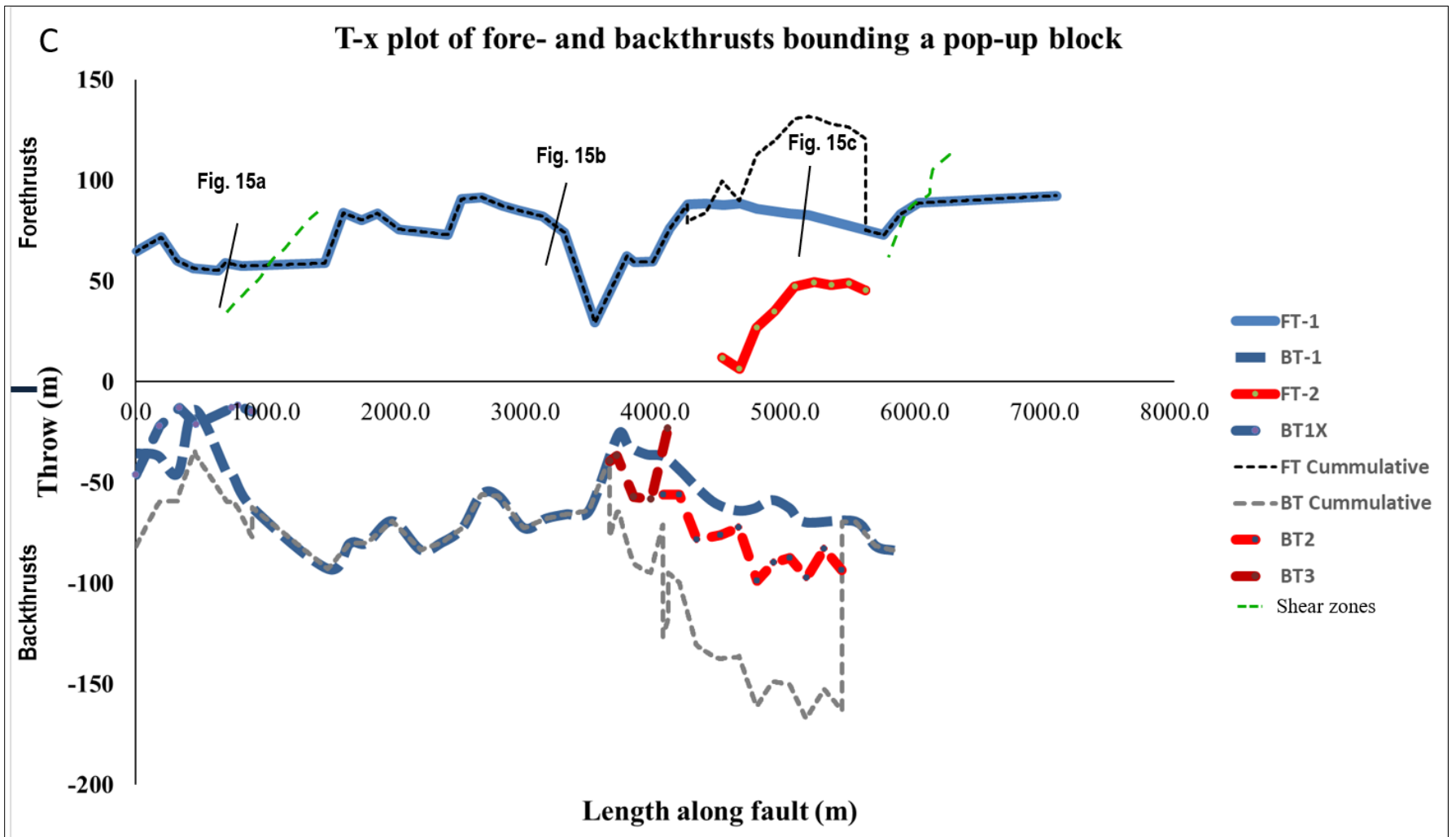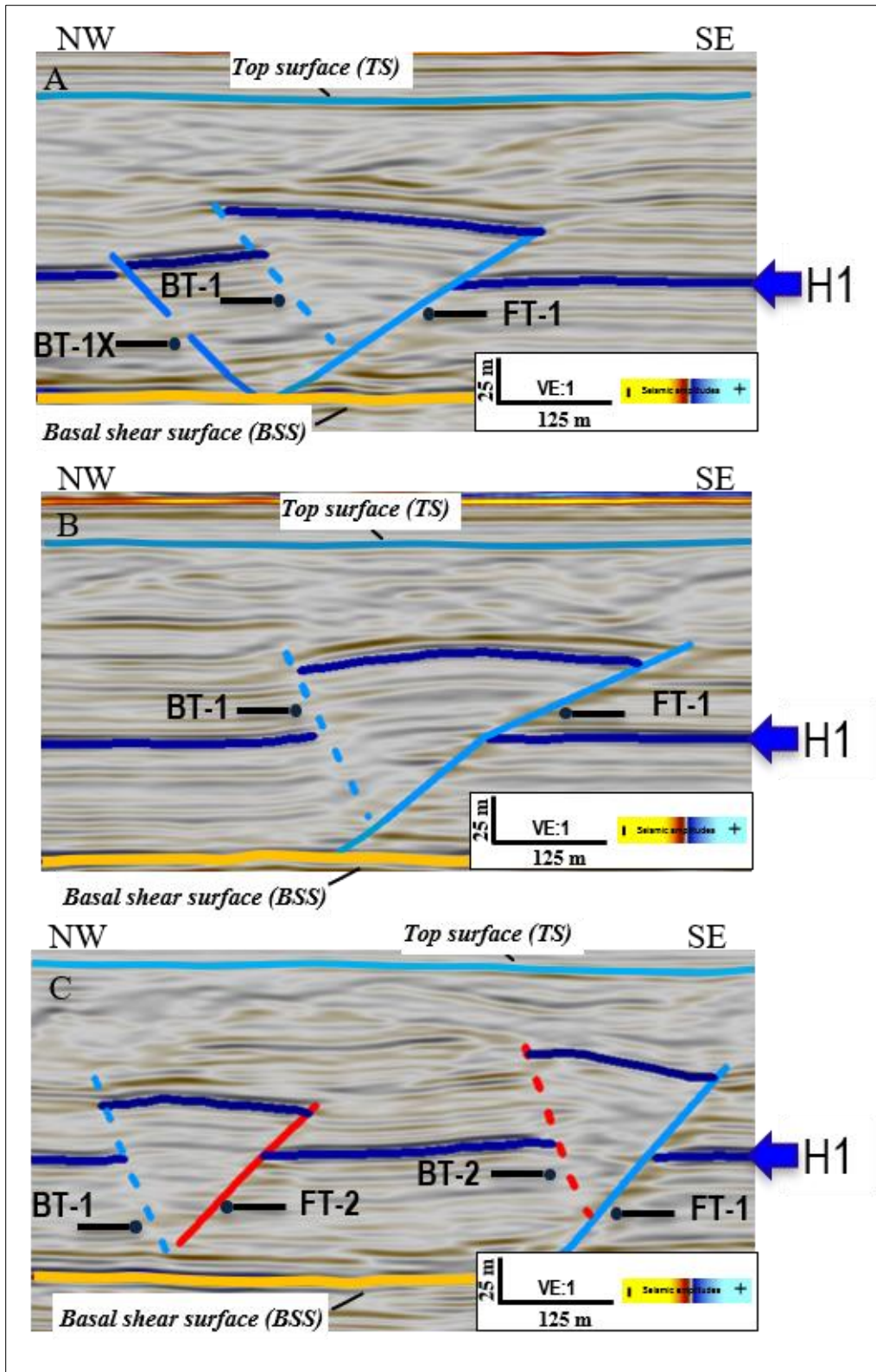
Figure 14

Figure 15
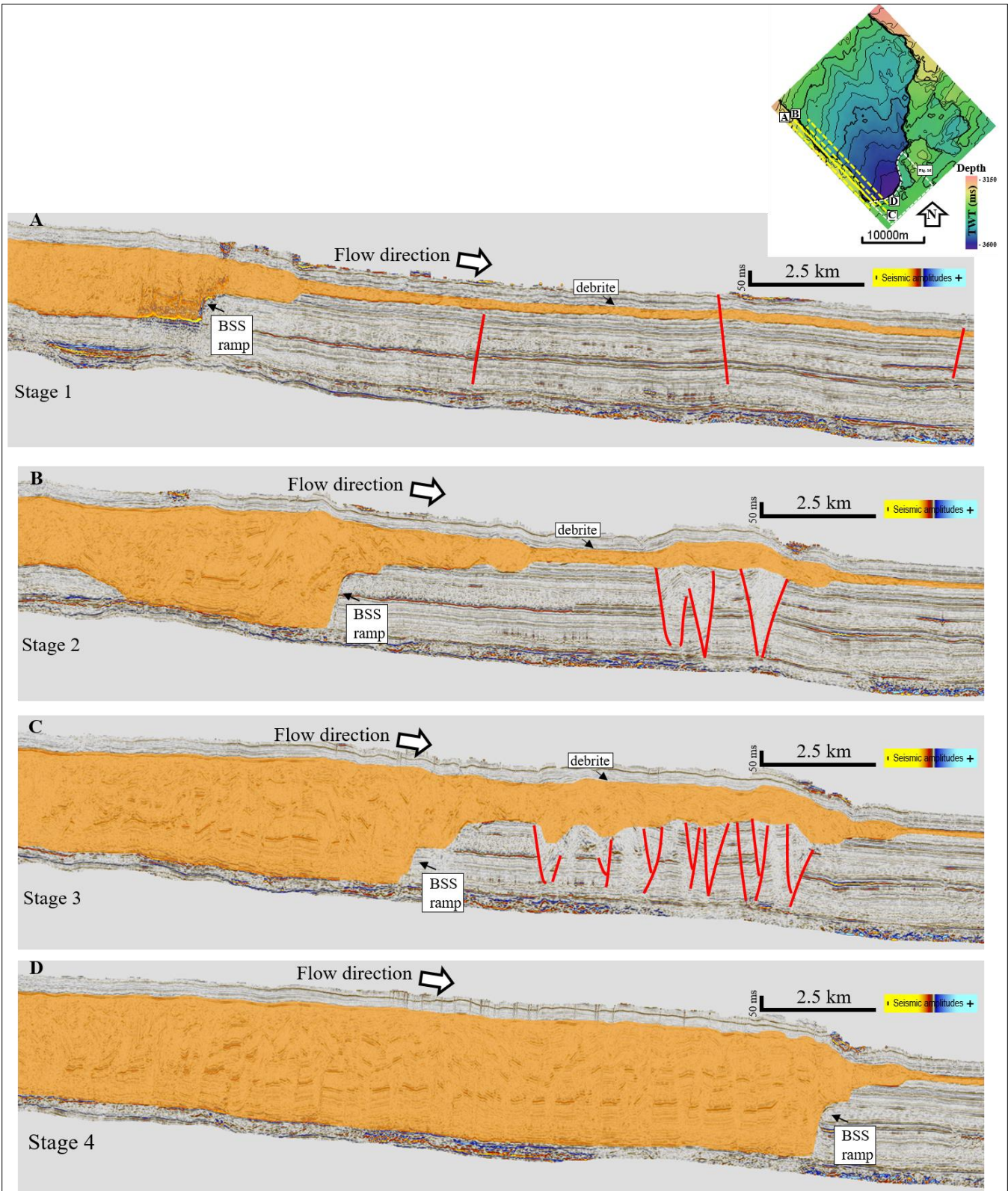
Figure 16
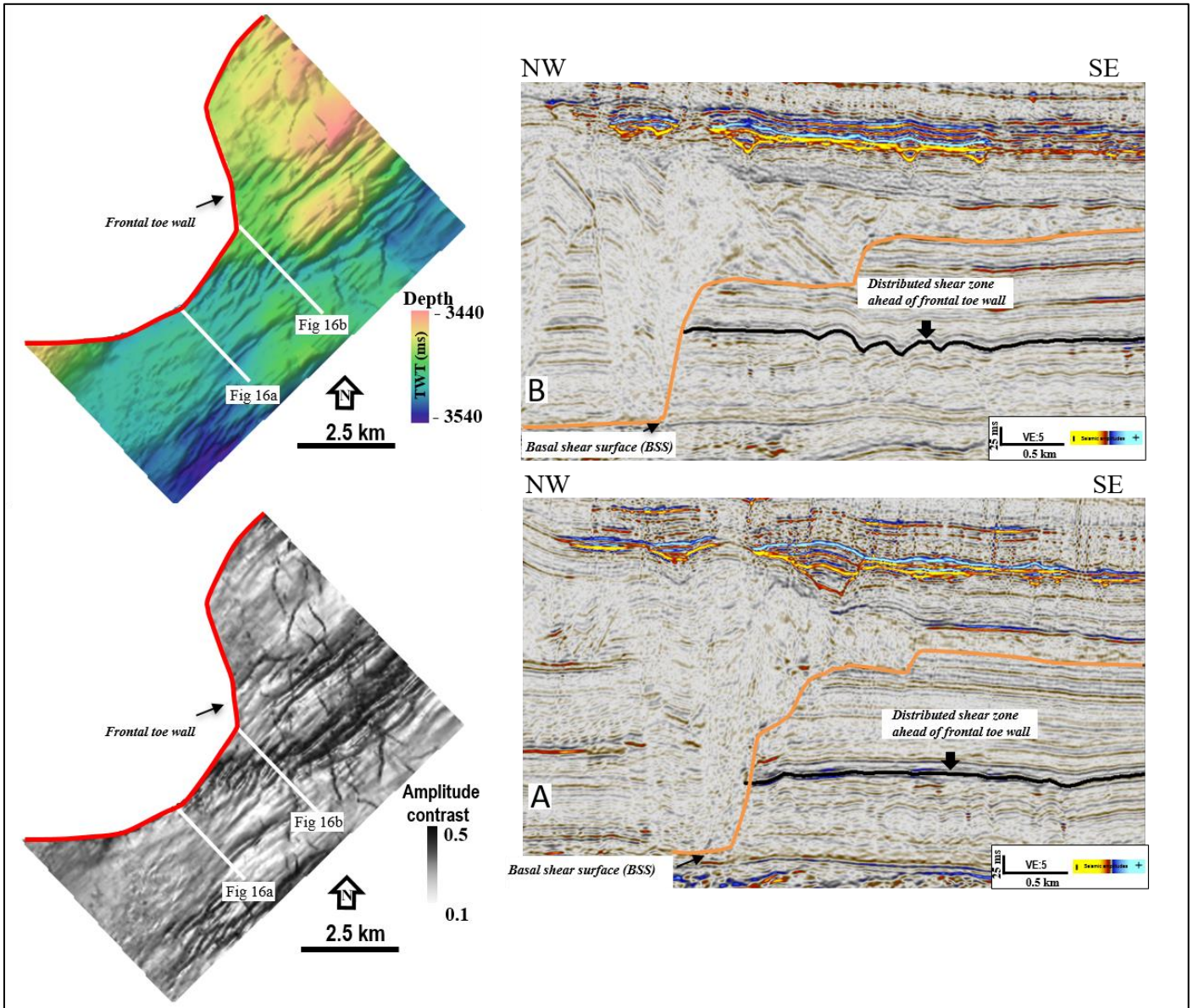
Figure 17
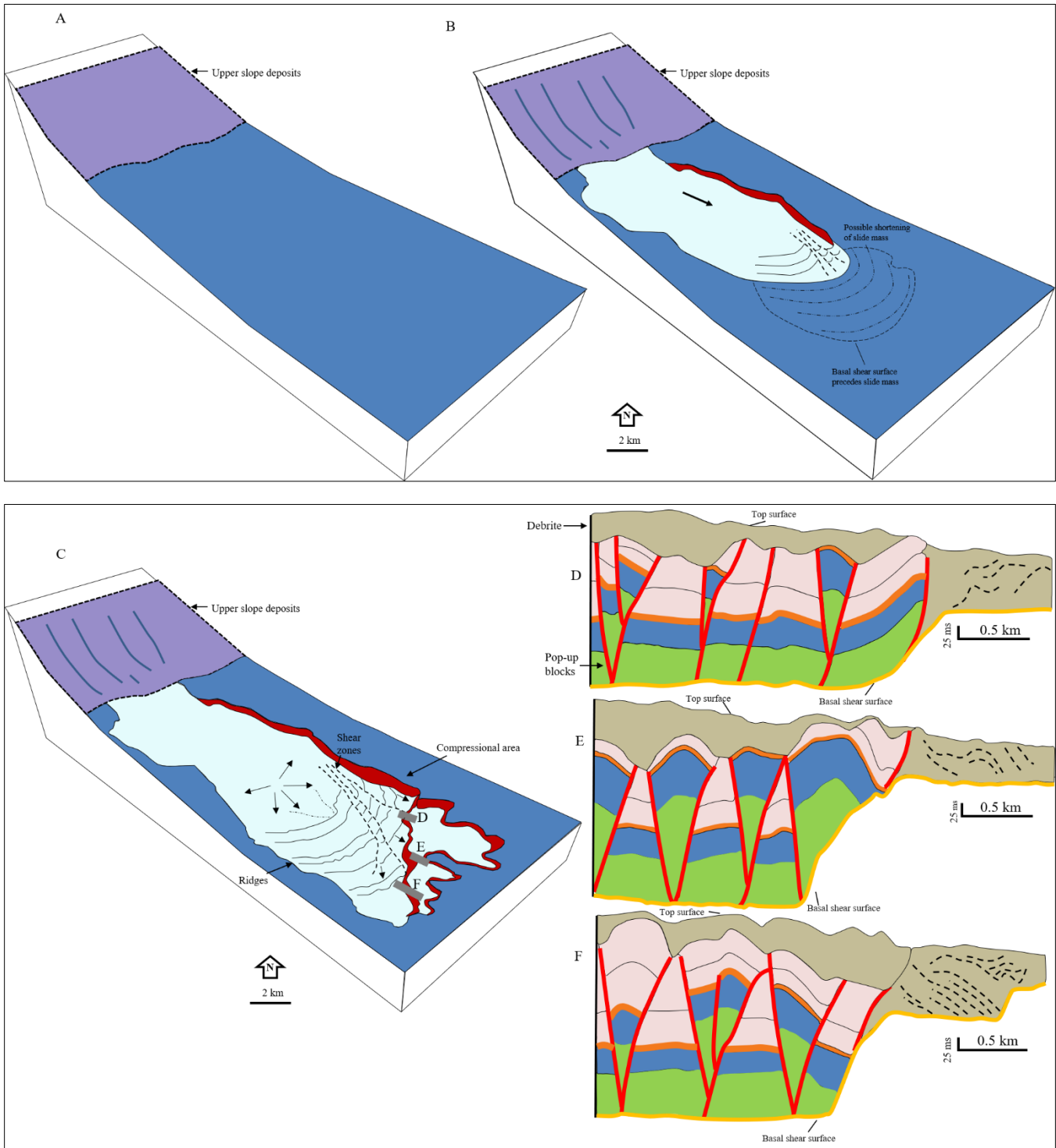
Figure 18

| A | Facies | Description | Interpretation |
|---|--------|-------------|----------------|
| | SF-1 | Very low-amplitude, chaotic reflections. Form c. 50% of the slide body. | Debritic matrix of the slide. Formed due to the disaggregation of updip source sediment (e.g. Posamentier and Kolla 2003; Posamentier and Martinsen 2011; Sutton et al. 2011; Ortiz-Karpf et al. 2017; Nugraha et al. 2019) |
| | SF-2 | Variable to high-amplitude, continuous reflections, which are folded and offset by thrusts. | Interpreted as imbricate folds and thrusts. The RGB highlights a remarkable pattern of continuous NE-trending lineation's in map-view, corresponding to forethrusts and backthrusts. These thrusts occur in oppositely-dipping pairs that are regularly spaced (average 1.43 km) and have maximum displacements of up to ca. 65 m. The thrusts bound high-RGB bodies that represent folded reflections in the thrust hanging walls (e.g. Frey-Martínez et al. 2006; Bull and Cartwright 2019). |
| | SF-3 | High-amplitude isolated blocks of coherent, parallel, weakly-to-moderately folded reflections that are encased within SF1 and 2. | Inferred to be megaclasts encased within a debritic matrix (i.e. SF1 and 2) (cf. Lee et al. 2004; McGilvery and Cook 2004; Moscardelli et al. 2006; Dunlap et al. 2010; Jackson 2011; Hodgson et al. 2018). Alternatively, they have been interpreted as remnants or in situ substrate that are not moved within the parent flow (Bull et al. 2009). |

Table 1

| Attribute | Description | Vertical seismic | Time slice |
|-----------|-------------|------------------|------------|
| Variance | Isolates edges and discontinuities |  |  |
| Ant-tracking | Identify faults, fractures and linear anomalies |  |  |
| eXchroma | Continuous rendering of seismic in RGB colors to reveal internal geometry |  |  |
| Dip illumination | Reveals structural discontinuities as faults and surface rugosity |  |  |
| RMS amplitudes | Highlights isolated geologic features |  |  |
| Amplitude contras | Extracts and highlights structural features that are difficult to detect |  |  |
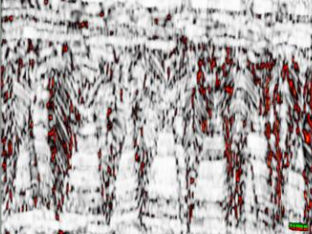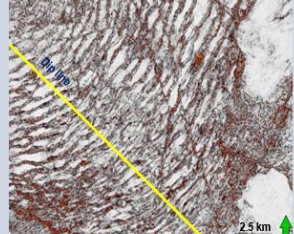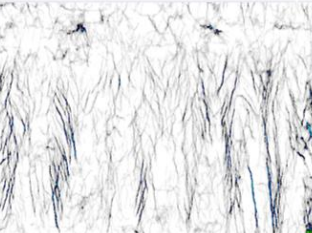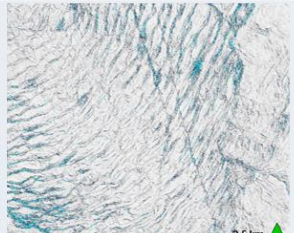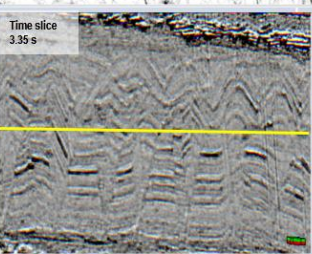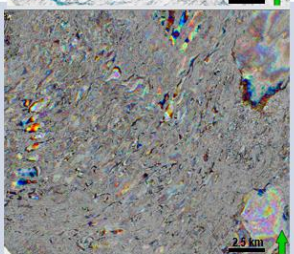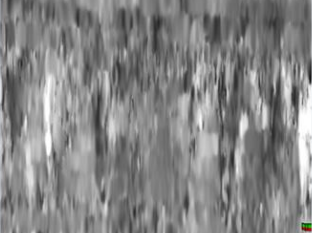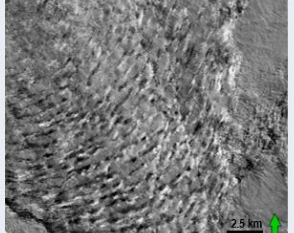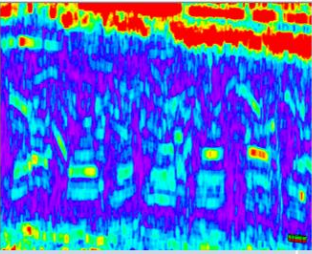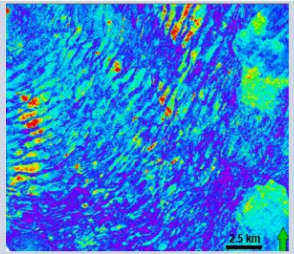
Appendix 1